EVALUATION OF ACID FRACTURING USING THE METHOD OF DISTRIBUTED VOLUMETRIC SOURCES

A Thesis

by

JAEHUN LEE

Submitted to the Office of Graduate Studies of
Texas A&M University
in partial fulfillment of the requirements for the degree of

MASTER OF SCIENCE

August 2009

Major Subject: Petroleum Engineering

EVALUATION OF ACID FRACTURING USING THE METHOD OF DISTRIBUTED VOLUMETRIC SOURCES

A Thesis

by

JAEHUN LEE

Submitted to the Office of Graduate Studies of
Texas A&M University
in partial fulfillment of the requirements for the degree of

MASTER OF SCIENCE

Approved by:

Chair of Committee,	Peter P. Valkó
Committee Members,	Christine Ehlig-Economides
	Guido Kanschat
Head of Department,	Stephen A. Holditch

August 2009

Major Subject: Petroleum Engineering

ABSTRACT

Evaluation of Acid Fracturing Using the Method of Distributed Volumetric Sources. (August 2009)

Jaehun Lee, B.S., Hanyang University, South Korea

Chair of Advisory Committee: Dr. Peter P. Valkó

Acid fracturing stimulation is one of the preferred methods to improve well productivity in carbonate reservoirs. Acid is injected into the fractured zone after a starter fracture is created in the near wellbore area by viscous fluid (pad). This results in propagation of a two-wing crack away from the perforations with simultaneous dissolution etching of the created surfaces. If the created etched surface is non-uniform, then after the treatment ends and the fracture face closes, a high conductivity path may remain in the formation, connected to the well. The important factors controlling the effectiveness of acid fracturing are the etched-fracture penetration and conductivity.

In this research, I use the distributed volumetric sources (DVS) method to calculate gas production from a well stimulated by acid fracturing. The novel concept realized in this research is that, during the production process, the conductivity of the acid created fracture changes. I use the Nierode - Kruk correlation to describe this effect as a function of effective closure stress that in turn is determined from the flowing bottomhole pressure and minimum horizontal stress. By combining the well productivity calculation from the DVS method taking into account varying fracture conductivity with gas material balance, I obtain an improved model of gas production. The model is then used to not only forecast production from acid fractured wells but also to evaluate the known

production history of such wells. Based on the concepts discussed above, I have developed a program called “Gas Acid” which is useful to optimize acid fracturing treatments and also suitable to infer created fracture parameters from known production history. The “Gas Acid” program has been validated with data from two Saudi Aramco gas wells.

It was found that the production forecast obtained from the “Gas Acid” program matches the actual production history with reasonable accuracy and the remaining discrepancy could be resolved by taking into account refinement of the material balance. The refinement became necessary, because the “Gas Acid” program was developed for dry gas but the reservoir fluids in the field examples were classified as retrograde gas and wet gas. When accounting for the additional mass of gas “hidden” in the produced condensate, the match of forecast and actual data was improved considerably.

DEDICATION

To my family and my fiancée Christy.

ACKNOWLEDGMENTS

I would like to express my sincere gratitude and appreciation to my advisor and committee chair, Dr. Peter P. Valkó, for believing in me and giving me continuous technical advice and creative ideas in completing this work.

I would also like to thank Dr. Christine Ehlig-Economides and Dr. Guido Kanschat for serving as my committee members.

Finally, I would also like to thank all my officemates and classmates for their friendship and my thanks go to Texas A&M University for the quality education that I have received.

TABLE OF CONTENTS

CHAPTER Page

LIST OF FIGURES

FIGURE Page

FIGURE Page

LIST OF TABLES

CHAPTER I

INTRODUCTION

1.1 Introduction

Acid fracturing is one of the fundamental methods for enhancing hydrocarbon recovery of a carbonate formation. It is well known that acid fracturing is a successful method for a heterogeneous formation. Hydrochloric acid is generally used to create an etched fracture surface, which is the main reason for maintaining a partially open fracture during the life of a well (Abass *et al*., 2006). If the created etched surface is non-uniform, then the fracture may sustain a high conductivity path to the wellbore after closure, because the resulting width will be zero only at discrete point locations. The important factors increasing the effectiveness of acid fracturing are the etched-fracture length and the resulting fracture conductivity. However, it is difficult to estimate fracture length and fracture conductivity for various reasons.

I have used the Nierode-Kruk correlation as a conservative way to estimate fracture conductivity in my research and have left fracture length as a design parameter. The distributed volumetric sources (DVS) method is used to calculate well productivity (from constant-rate pressure response) and, by combining the well productivity with gas material balance, production forecasting is available. Based on the above ideas, I developed a program which can estimate the performance of acid fractured wells. Furthermore, the program can be easily applied to determine optimum treatment parameters resulting in maximum production under various technical and economic constraints.

This thesis follows the publication style of *SPE Journal.*

1.2 Objectives

The objectives of this study are to build an acid fracturing performance program (called Gas Acid) which calculates the productivity of the acid fractured reservoir and to validate the program using field data. The main advantages of using "Gas Acid" are stated as below:

- The program provides dimensionless productivity index (PI), flow rate, cumulative production, average reservoir pressure for a given reservoir geometry and the well completion scheme.
- Based on the simulated performance data, we are able to optimize treatment size and fracture dimension to maximize productivity achievable with given acid volume.
- A proper stimulation method in carbonate reservoirs can be selected by using both a proppant fracturing program called "Gas 14" developed by Dr. Valko *et al*. and an acid fracturing program (Gas Acid).

CHAPTER II

LITERATURE REVIEW

2.1 Acid Fracturing vs. Proppant Fracturing

The primary difference between acid fracturing and proppant fracturing is that different methods are used to maintain fracture conductivity after the fracture closes (Kalfayan, 2007): an etched pattern of voids on the fracture faces and propping the faces apart, respectively. In both cases, fracture height is principally controlled by the stress contrasts in bounding rock layers, and fracture length depends upon the height containment and the leak off properties of the fracturing fluid. In proppant fracturing, the fracturing gel can be penetrates deeper into the formation than in acid fracturing since the fracturing gel does not react with the formation. In general, acid-etched fractures are limited in penetration but can result in high conductivity whereas proppant fractures usually have a deeper penetration but may be conductivity limited.

There are no sets of guidelines for choosing between acid fracturing and proppant fracturing. Historically the choice has been mostly based on logic and experience with previous treatment response in the same field under conditions that might be considered similar. However, knowledge of formation conditions can provide guidance for choosing the type and the size of the stimulation treatment method. Factors more favorable to proppant fracturing treatment in carbonate include (Economides *et al*., 1998):

- Acid (HCl) solubility is low (< 65-75%).
- The carbonate formation is relatively homogeneous (e.g., pure limestones).
- Acid reactivity is low (lower temperature dolomites; < 150 °F).
- Formation permeability is very low – thus requiring long fracture length.

- The rock softens or creeps significantly under closure after contact with acid – resulting in poor retention of acid-etched fracture conductivity.
- The formation has very high closure pressure – resulting in unsustainable acid-etched fracture conductivity.

Factors more favorable to acid fracturing treatment in carbonate include :

- The carbonate formation is predominately naturally fractured – which could lead to complications in case of proppant fracturing.
- The formation is heterogeneous with porosity and permeability streaks that are conducive to a higher degree, enabling differential acid-etching of the fracture walls.
- Zone of interest is in close proximity to unwanted water or gas zone(s) not separated by stress barrier(s).
- Formation permeability is relatively high and/or near wellbore formation damage exists.
- The well will not mechanically accept proppant.

2.2 Acid Etched Fracture Conductivity

Acid fracture conductivity is one of the factors controlling the effectiveness of acid fracturing (Economides *et al*., 1998). However measurements of acid-etched conductivity in the laboratory are usually not reproducible or representative of large-scale in-situ behavior because of heterogeneities in the rock and the small size of laboratory samples. This makes difficulties in calculation and validation of acid-etched fracture conductivity.

2.2.1 Nireode and Kruk Correlation

The most reliable method to estimate acid fracture conductivity was presented by Nierode and Kruk (1973). The created fracture conductivity, $k_f w$ (md-ft), can be calculated using ideal fracture width, w_i (in.), rock embedment strength, S_{rock} (psi), and the net closure pressure, σ (psi):

$$w_i = \frac{12XV}{(1-\phi)2h_f x_f} \quad \text{..... (2.1)}$$

$$k_f w = C_1 e^{-C_2 \sigma} \quad \text{..... (2.2)}$$

$$C_1 = 1.47 \times 10^7 w_i^{2.47}$$
$$C_2 = (13.9 - 1.3 \ln S_{rock}) \times 10^{-3} \quad \text{if } S_{rock} < 20{,}000 \text{ psi}$$
$$C_2 = (3.8 - 0.28 \ln S_{rock}) \times 10^{-3} \quad \text{if } S_{rock} > 20{,}000 \text{ psi}$$

The ideal fracture width, w_i, can be obtained by calculating the volume of rock dissolved by the acid and dividing by the fracture area. Here X is the volumetric dissolving power of the acid and V is the injected acid volume. h_f is fracture height and x_f is fracture half length. The C_1 term is related to the ideal fracture width. The C_2 term is related to rock embedment strength. The rock embedment strength has to be determined experimentally from core or outcrop samples. Extensive library data for S_{rock} is available for many of the more commonly fractured carbonate formations. **Fig. 2.1** shows a hypothetical diagram for the net closure stress on the fracture faces which is a result of the minimum horizontal stress against flowing bottomhole pressure.

The experimental studies show that the effect of rock heterogeneity is very important. Interesting observations relevant to stimulation of carbonate reservoirs have

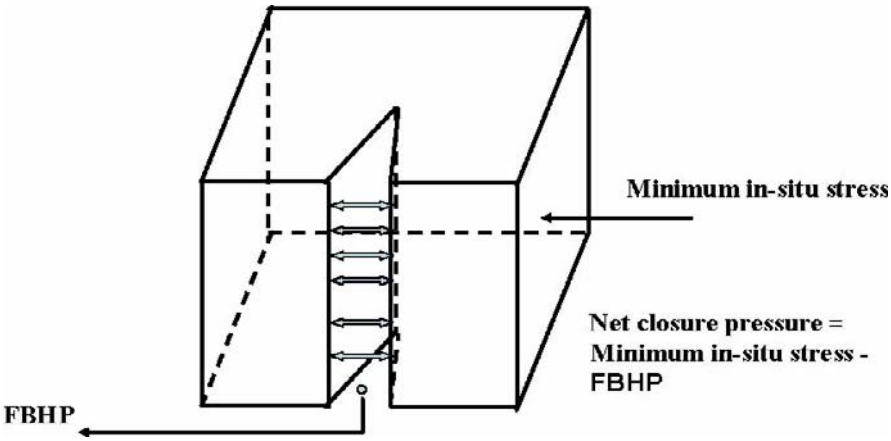

Fig. 2.1-The physical meaning of the net closure stress which was used in Nierode-Kruk correlation (Algahmdi, 2005).

been reported in the literature. Fracture conductivity does not increase with increasing amounts of dissolved rock (Abass *et al*., 2006). Nierode-Kruk correlation was based on the principle that the larger the amount of rock dissolved, the larger the conductivity of the fracture. The Nierode-Kruk correlation has some contradictions with natural assumptions. However the Nierode-Kruk correlation is the most reliable way to estimate acid fracture conductivity in the present.

2.3 Fracture Closure in Acid Fracturing

Productivity increase due to an acid fracturing treatment is generated from two factors (Abass *et al*., 2006); fracture length and fracture conductivity. Fracture length is controlled by acid convection (injection rate), acid-reaction rate, and acid-loss rate. Fracture width is a result of the differential etching occurring as the acid reacts with the walls of the created fracture. This will create an uneven fracture surface that will determine the fracture width upon fracture closure. Therefore, fracture conductivity is determined by the amount of rock dissolved, fracture-surface roughness, closure stress,

and the stress-strain characteristics of rock formation. If reservoir temperature is too high, optimization of the injection rate becomes very critical to create a long conductive fracture. If the reaction rate is low, uniform etching may be resulted leading to insufficient fracture conductivity. The industry has focused on reducing fluid loss and acid reaction by increasing acid viscosity such as using emulsified and gelled acid systems. Upon completion of an acid fracturing treatment, three factors will contribute to a reduction in fracture conductivity (Abass *et al*., 2006):

a. Elastic response
b. Compressive failure of contact point (asperities)
c. Creeping effect

The elastic closure response occurs when the net effective minimum horizontal stress increases as a result of reservoir depletion. The elastic response to close the fracture follows Hooke's law of elasticity and it is controlled by Young's modulus of the formation. The elastic response will decrease the aperture of the fracture which reduces fracture conductivity. The compressive strength of the asperities will determine the severity of their failure on fracture permeability. The reduction in conductivity is due to a combined effect of elastic response and compressive failure of the asperities. Compressive failure also generates rock particles and fines that will further reduce fracture conductivity. The creeping (viscous) effect is a slow time dependant displacement. Experiment for creeping effect has been conducted by Abass *et al.* (2006). They concluded that creeping test is introduced to provide additional criterion to make decision on selecting a proppant or acid fracturing treatment for a given formation and in-situ conditions.

2.4 Dimensionless Productivity Index and Dimensionless Fracture Conductivity

A well in a reservoir developed on a certain pattern has a finite drainage area (Economides *et al*. 2007). During most of its lifetime, it is producing in a stabilized flow regime called pseudo-steady state (or more precisely, boundary-dominated state). During the stabilized flow regime, the productivity index of a well (PI), defined by the production rate divided by the pressure drawdown, is calculated as:

$$J = \frac{q}{\bar{p} - p_{wf}} \quad \text{..... (2.3)}$$

The dimensionless productivity index, J_D, is defined as

$$J_D = \frac{\alpha_1 B\mu}{kh} J \quad \text{..... (2.4)}$$

For an unstimulated well in a circular reservoir, J_D is given by the well-known formula:

$$J_D = \frac{1}{\ln(0.472\frac{r_e}{r_w}) + s} \quad \text{..... (2.5)}$$

with the skin factor, s, representing deviation from the base case (without any near-wellbore damage or stimulation).

For a fracture stimulated well, J_D is affected by the volume of proppant placed into the pay layer, by the permeability ratio of the proppant bed and the reservoir, and by the geometry of the created fracture (Economides *et al*., 2002). All these factors can be characterized by two dimensionless numbers-the dimensionless fracture conductivity, C_{fD}, and the penetration ratio, I_x :

$$C_{fD} = \frac{k_f w}{k x_f} \quad \text{..... (2.6)}$$

$$I_x = \frac{2x_f}{x_e} \quad \text{..... (2.7)}$$

The combination of the two dimensionless numbers is the dimensionless proppant number :

$$N_{prop} = I_x^2 C_{fD} = \frac{4k_f x_f w}{kx_e^2} = \frac{4k_f x_f wh}{kx_e^2 h} = \frac{2k_f}{k}\frac{V_p}{V_r} \quad \text{.....} \quad (2.8)$$

Where V_p is the proppant fracture volume contained within the pay zone and V_r is the drained volume of the pay (in short, the well drainage volume). The dimensionless proppant number is the appropriate way to express the relative size of a given treatment. In other words, N_{prop} represents in a dimensionless form the amount of resources spent on the treatment. Algorithms are available to calculate dimensionless productivity index as a function of C_{fD} with N_{prop} as a parameter. Valkó and Economides also found that for a given value of N_{prop}, there is an optimal dimensionless fracture conductivity at which the productivity index is maximized. Typical results are shown in **Fig. 2.2** and **Fig. 2.3**.

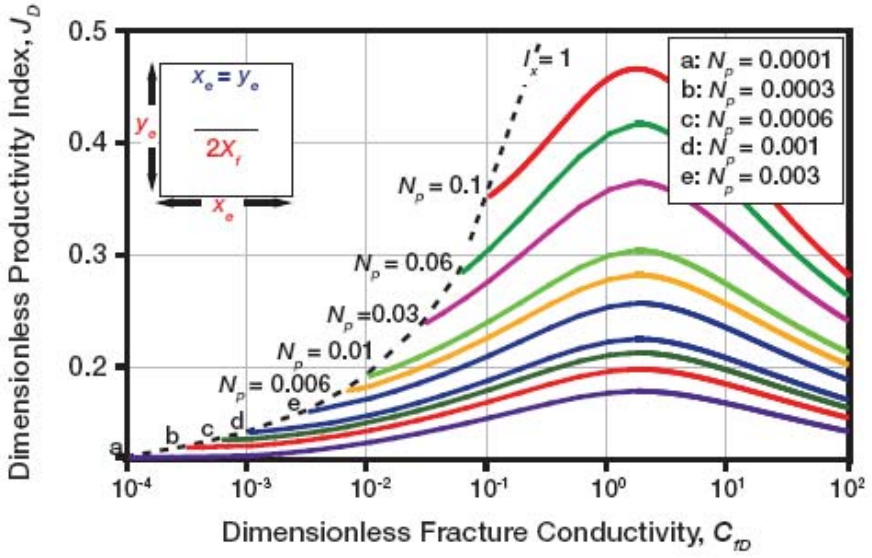

Fig. 2.2—Dimensionless productivity index as a function of dimensionless fracture conductivity with proppant number as a parameter for $N_{prop} \leq 0.1$

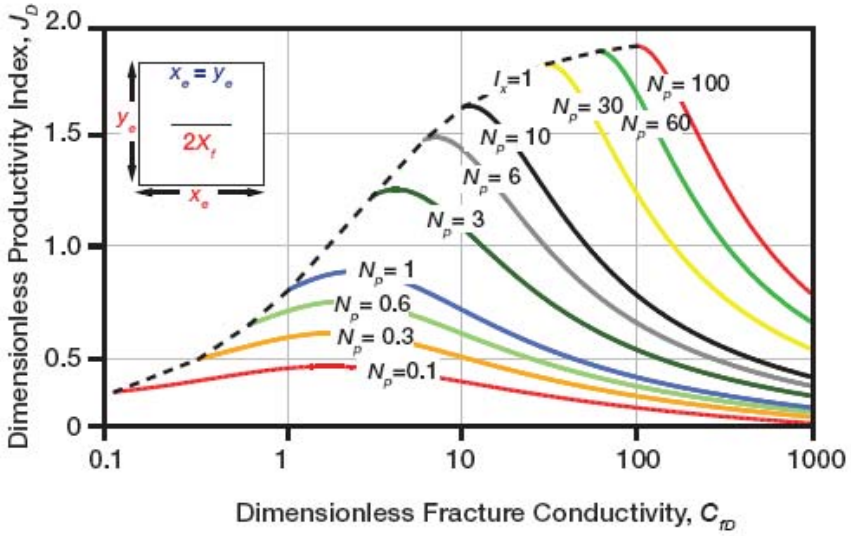

Fig. 2.3—Dimensionless productivity index as a function of dimensionless fracture conductivity with proppant number as a parameter, for N_{prop}>0.1

As explained previous section 2.2.1, acid fracture conductivity is obtained with Nierode-Kruk correlation. The obtained acid fracture conductivity can be used in the expression of dimensionless fracture conductivity instead of the product $k_f w$. Therefore, using the penetration ratio I_x, an equivalent proppant number can also be calculated using Equation 2.8; consequently optimal dimensionless fracture conductivity concept is readily applicable.

2.5 Infinite-Acting Flow and Boundary-Dominated Flow

Flow in a reservoir is often characterized as being one of two types, namely transient or boundary-dominated (Fekete Associates Inc, 2005). Transient flow takes place during the early life of a well, when the reservoir boundaries have not been felt, and the reservoir is said to be infinite-acting. During this period, the size of the reservoir has no effect on the well performance, and from analysis of pressure or production, nothing

can be deducted about the reservoir size. In theory, the size of the reservoir does have an effect even at very early times, but in reality, this effect is so small as to be negligible and not quantifiable with any kind of confidence. Transient flow forms the basis of a domain of reservoir engineering called Pressure Transient Analysis, also known as well test interpretation.

The field of well testing relies heavily on equations of flow for a well flowing at constant rate. Initially, the flow regime is transient but the well will flow at steady state eventually when all the reservoir boundaries have been felt, if a constant pressure boundary exists, or at pseudo-steady state, if all the boundaries are no-flow boundaries. During pseudo-steady state, the pressure throughout the reservoir declines at that same rate as shown in **Fig. 2.4**, and the reservoir acts like a tank (hence the alternative name, tank-type behavior). The concept of pseudo-steady state is applicable to a situation where the well is flowing at a constant flow rate.

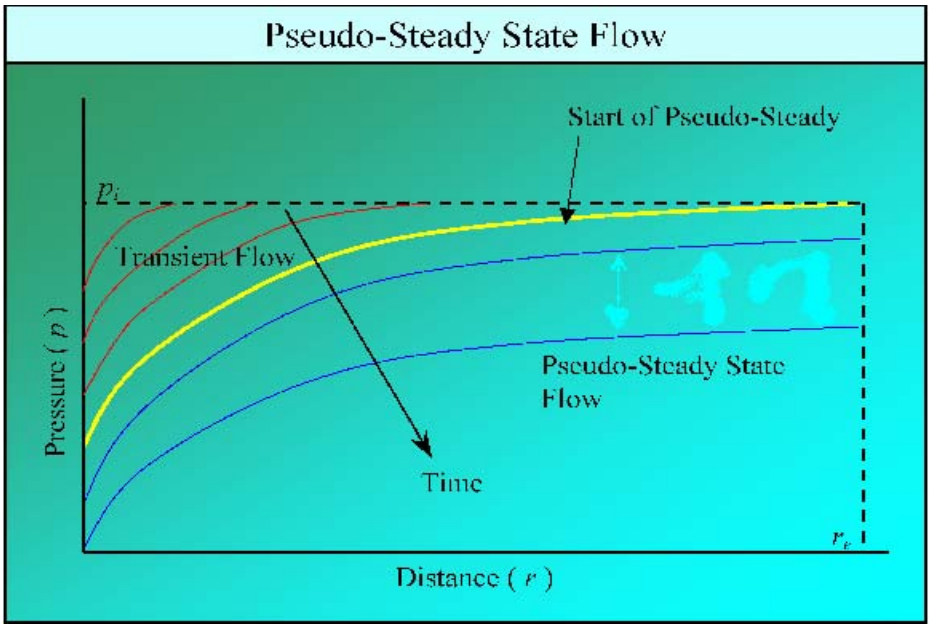

Fig. 2.4—Transient flow and pseudo-steady state flow profile in a tank reservoir model (Fekete Associates Inc, 2005)

When a well is flowing at a constant flowing well-bore pressure, as is often the case in production operations, there is a period of time during which boundaries have no influence, and the flow behavior is "transient". However, after a period of time, when the radius of investigation has reached the outer boundary, the boundary starts to influence the well performance, and the pressure drops throughout the reservoir. But unlike pseudo-steady state flow, where the pressure drop is uniform throughout the reservoir, the pressure at the well is kept constant and the pressure at the boundary is dropping due to depletion. This is a case where the boundary is affecting the reservoir pressure, and hence the production rate, but it cannot be called pseudo-steady state, because the pressure drop in the reservoir is not uniform, so it is called boundary-dominated flow as shown in **Fig. 2.5**. Thus, boundary-dominated flow is a generic name for the well performance when the boundaries have a measurable effect. Pseudo-steady state flow is only one type of boundary-dominated flow, which takes place when the well is flowing at a constant rate.

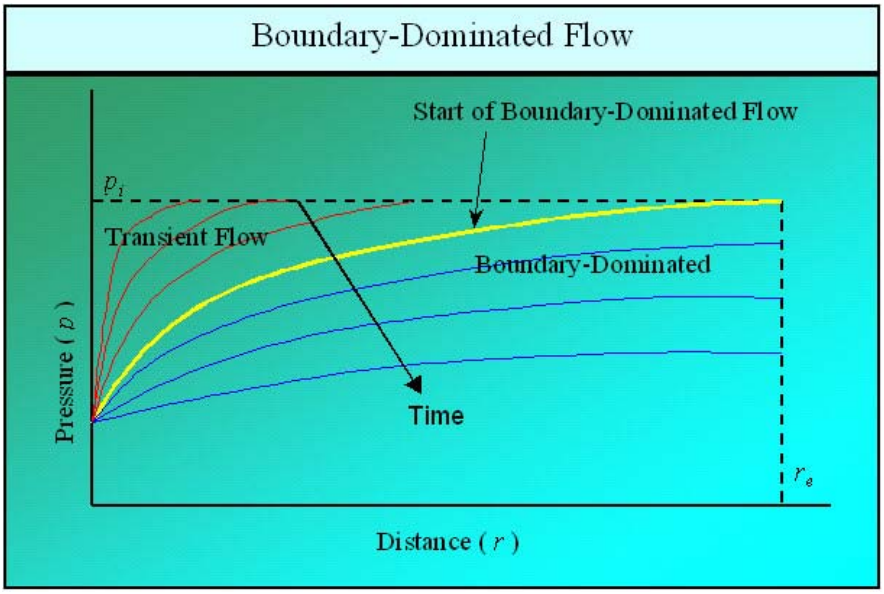

Fig. 2.5—Transient flow and boundary-dominated flow profile in a reservoir model (Fekete Associates Inc, 2005)

CHAPTER III

METHODOLOGY

3.1 The Distributed Volumetric Sources Method

3.1.1 Introduction to DVS Method

In a rectilinear reservoir model, the Distributed Volumetric Sources (DVS) method was initially developed by Valko and Amini (2007) to express pressure response analytically for a volumetric source. In this method, not only an oil/gas reservoir is modeled as a rectilinear shape with closed boundaries for simplicity in describing reservoir but also the source is described as a box-volumetric source inside of the rectilinear shaped reservoir. In modeling a reservoir and its source as a box-in-box model, we are able to find pressure response with analytical method in transient and pseudo steady state flow conditions. As Amini (2007) discussed in his dissertation, the solution also provides the well-testing derivative of the response to a continuous source in analytical form and the derivative can be integrated over the time to provide the pressure response to a continuous source. Since the most interest in the oil industry is optimizing production by studying reservoir behavior, the calculated pressure response in a box-in-box model will be used to determine productivity index of a reservoir over the time period. Consequently, this integrated reservoir modeling and PI calculations allow us to predict future production by combining productivity index with material balance and to detect abnormal behavior of reservoir or near wellbore area in more accurate manner. In addition, the DVS mehthod manages different types of well configurations, but this will not be discussed in this paper as no deviated wells were studied for acid treatment through my research.

3.1.2 Pressure Response for Finite Conductivity Case

The first step of the DVS method is to develop the pressure response of a rectilinear reservoir with closed boundaries to an instantaneous withdrawal from the source. A porous media is assumed to be an anisotropic and homogeneous reservoir shaped as a box. The box is oriented in line with the three principal directions of the permeability field. The source is assumed to be an inner rectilinear box with its top paralleled to the reservoir boundaries. It is assumed to have the same media properties as the reservoir. **Fig. 3.1** shows the schematic of the system. The instantaneous unit withdrawal is distributed uniformly in the volume of the source. In short, we will refer to the solution as instantaneous source response of the box-in-box and will denote the response observed at a location (x_D, y_D, z_D) as $p_{\delta D}(box-pars; x_D, y_D, z_D, t_D)$. The box-pars notation stands for all the information contained in the problem specification: (x_e, y_e, z_e, k_x, k_y, k_z, c_x, c_y, c_z, w_x, w_y, w_z). For the meaning of the variables, see **Fig. 3.1**.

The result is obtained from Newman's principle as

$$p_{\delta D}(box-pars; x_D, y_D, z_D, t_D) = f(x-pars; x_D, t_{Dx}) \times f(y-pars; y_D, t_{Dy}) \times f(z-pars; z_D, t_{Dz}) \quad \text{..... (3.1)}$$

where $f()$ represents the solution of a 1D problem with the source distributed along a finite section of the "linear" reservoir. The structure of Eq. 3.1 already indicates that anisotropy is handled in the parameters of the 1D solution. This comprises the main advantage of the DVS method; once an effective method is available to accurately calculate $f()$, the additional programming requirement is minimal. The details are provided by Valkó *et al*. (2007).

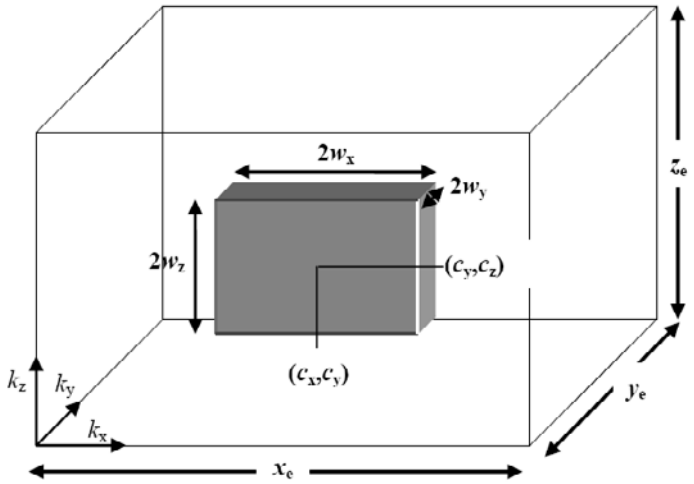

Fig. 3.1—Schematic of the box-in-box model

To obtain the response of the reservoir to a continuous unit source distributed uniformly in the small box, we numerically integrate the solution, Eq. 3.1 over time:

$$p_{uD}(x_D, y_D, z_D, t_D) = \int_0^{t_D} p_{\delta D}(x_D, y_D, z_D, \tau) d\tau \quad \text{..... (3.2)}$$

To obtain wellbore flowing pressure, we need to calculate $p_{uD}(x_D, y_D, z_D, t_D)$ at the geometric center of the well. The instantaneous source solution (which is equal to the well testing pressure derivative function), $p_{\delta D}(x_D, y_D, z_D, \tau)$ and the continuous source solution (which is the well testing pressure function), $p_{uD}(x_D, y_D, z_D, t_D)$ can be used as type-curves for pressure transient analysis.

In the DVS method the time integration in Eq. 3.2 is done numerically. Notice that while the 1D instantaneous responses could be easily integrated analytically over time, the same cannot be said for their product. On the other hand, the Newman principle can be applied to the instantaneous response but not to the continuous unit response. Whether the actual well/fracture configuration is represented by one or more such volumetric sub-sources, the pressure has to be calculated at the geometric center of the

sub-source. Since the singularity is removed in this method, we do not need to select an arbitrary point on the surface of the source or outside it. In the general case, *n* sub-sources are used to represent a certain well/fracture configuration and the total pressure response at any point of the reservoir is calculated by superposition in space:

$$p_{Dr} = \sum_{j=1}^{n} q_{Dj}\, p_{Dr,j} \quad \text{..... (3.3)}$$

It should be noted that $p_{Dr,j}$ in Eq. 3.3 stands for the pressure change effect of the sub-source *j* measured at the center of the r^{th} sub-source and is calculated using Eq. 3.2 with the source coordinates of the j^{th} and observation point coordinates of the r^{th} sub-source. In Eq. 3.2 the source strengths, q_{Dj} are usually not known a priori. They have to be determined simultaneously from some additional criterion describing pressure relations between the sub-sources. For instance, to describe an infinite conductivity source system, one adds *n* requirements: assuring the calculated pressure at the geometric center of each sub-source is equal to the same yet unkown pressure: p_{Dw}. The *n* equations are obtained by writing Eq. 3.3 for k=1…n points being in the geometric center of the sub-sources. The n equations together with the requirement for the sum of strengths being equal to unity allow the simultaneous determination of the $n+1$ unknowns: q_{Dj} and p_{Dw}. In general, we write

$$Aq_D + Cq_D = p_{Dw} \quad \text{..... (3.4)}$$

where q_D is the *n*-vector of strengths and p_{Dw} is the *n*-vector having the wellbore reference pressure as each of its component.

The physical meaning of the *k*-th row of Eq. 3.4 is quite straightforward. First the effect of all sub-sources is summed up, thereby obtaining the pressure at the geometric center of the *k*-th sub-source. Therefore, the elements of the $n \times n$ **A** matrix are the $p_{Dk,j}$

pressures calculated from Eq. 3.2. The A matrix is time dependent and we prefer to look at it as a matrix with elements consisting of functions of time.

The additional terms in the *k*-th row of Eq. 3.4 represent pressure drops between the geometric center of the *k*-th sub-source and the well reference point. Therefore, the elements of the n x n **C** matrix are calculated as the pressure drop solutions of a flow problem within the source. The *k,j* element is the pressure drop between the geometric center of the *k*-th sub-source and the wellbore reference point, caused by the *j*-th inflow. In general, we can obtain the *j*-th column of the **C** matrix by solving a steady-state flow problem (within the source) with steady distributed inflow block j and outflow at the wellbore block. The row and column of the **C** matrix corresponding to the wellbore reference sub-source is identically zero since the inflow into this sub-source is taken out at the same place. A system of sub-sources connected in an infinite conductivity manner results in a zero **C** matrix. Such a system can be used to represent an infinite conductivity vertical fracture (with full or partial vertical penetration) or an infinite conductivity vertical or horizontal well.

Taking into account pressure drop due to flow within the source leads to non-zero **C** matrix. If the flow problem within the source can be considered as 1D, the construction of the **C** matrix is a relatively easy exercise. Such is the case for a finite conductivity vertical fracture of full vertical penetration if it is intersected by a vertical well. For more complex well/fracture configurations, the construction of the **C** matrix might require the solution of n 2D flow problems within the source. Such is the case if a finite conductivity vertical fracture is transversely intersected by a horizontal well.

If the flow problem within the source is linear, we need to calculate the **C** matrix only once. If the flow problem is nonlinear, the **C** matrix cannot be calculated a priori, but its determination is part of the solution procedure.

In my research, I considered the vertical well with a finite conductivity vertical fracture of fully vertical penetration so the source can be considered as 1D and linear.

3.1.3 Productivity Index Calculation

The application of DVS method is not limited to prediction of the pressure behavior of well/fracture configurations (Amini, 2007). The pressure data calculated from the method can be used to predict the productivity index (PI) behavior of the system. Equation 3.5 shows how to calculate the dimensionless productivity index of a system using the dimensionless pressure and time data. Detailed derivation of this equation is presented in Appendix B.

$$J_D = \frac{1}{P_{D,trad} - 2\pi t_{DA}} \quad \text{..... (3.5)}$$

3.2 Estimation of Acid Fracture Conductivity

As mentioned in the previous chapter (section 2.2), it is difficult to estimate acid fracture conductivity. Although much laboratory testing has been conducted, none has proven to be highly reliable. In my research, therefore, I used the Nierode and Kruk correlation, which is presently the most reliable correlation and a conservative estimate of acid fracture conductivity. In acid fracturing, conductivity depends heavily on the net closure stress acting on the fracture walls. In some parts of the world, gas wells are producing gas with relatively high flowing bottomhole pressure and only later in the life of the well is the flowing bottomhole pressure decreased, step by step, to its minimum value. To calculate acid fracture conductivity using the Nierode and Kruk correlation, one must specify inputs such as volumetric dissolving power, acid volume to be injected, minimum horizontal stress, rock embedment strength, and flowing bottomhole pressure. As flowing bottomhole pressure is changed over time, the acid fracture conductivity calculation should be repeated when each new flowing bottomhole pressure is established. Equations for acid fracture conductivity and calculation step are depicted in **Table 3.1**. Acid fracture conductivity is the most important factor which determines productivity of the well in simulation.

TABLE 3.1—Acid fracture conductivity calculation

1. Specify volumetric dissolving power, X and injected acid volume, V_i

$$X = \beta \frac{\rho_{acid\ solution}}{\rho_{mineral}}$$

2. Specify minimum horizontal stress, σ_{min} and rock embedment strength S_{rock}

3. Specify flowing bottomhole pressure p_{wf}

4. Calculate conductivity using the Nierode-Kruk correlation

$$w_i = \frac{XV}{(1-\phi)2h_f x_f}$$

$$k_f w = C_1 e^{-C_2 \sigma}$$

$$C_1 = 1.47 \times 10^7 w_i^{2.47}$$

$$C_2 = (13.9 - 1.3 \ln S_{rock}) \times 10^{-3} \quad \text{if } S_{rock} < 20{,}000 \text{ psi}$$

$$C_2 = (3.8 - 0.28 \ln S_{rock}) \times 10^{-3} \quad \text{if } S_{rock} > 20{,}000 \text{ psi}$$

5. Repeat steps 3-4 if p_{wf} is changed

3.3 Two Variable Interpolation for Dimensionless PI

In this study, fracture is described as vertical fracture with finite conductivity that can be easily calculated by the DVS method. The DVS method requires inputs such as reservoir properties, source properties to calculate pressure response of the reservoir and productivity index (see **Table 3.2**). In acid fracturing, it is not possible to estimate fracture width and fracture permeability separately or set as a design value. But acid fracture conductivity, which is the product of fracture width and fracture permeability, can be estimated using the Nierode-Kruk correlation. This requires adding more input

values such as acid properties and FBHP history and modifying input forms of reservoir properties and source properties (see **Table 3.3**).

TABLE 3.2—Inputs for calculation of productivity index in DVS method	
Reservoir properties	xe, reservoir length, ft
	ye, reservoir width, ft
	ze, formation thickness, ft
	kx, permeability along the reservoir length direction, md
	ky, permeability along the reservoir width direction, md
	kz, permeability along the reservoir height direction, md
Source properties	c_x, x-coordinate of the center point of fracture
	c_y, y-coordinate of the center point of fracture
	c_z, z-coordinate of the center point of fracture
	w_x, fracture half-length, ft
	w_y, fracture half-width, ft
	w_z, fracture half-height, ft
	k_f, average fracture permeability, md

Acid fracture conductivity can be calculated with added input data, but still, the productivity index cannot be calculated with the standard DVS method. To enable productivity calculation with variable fracture conductivity over time, we use two-variable interpolation. If other inputs are uniform, acid fracture conductivity ($k_f w$) is the only factor to affect productivity index with time. It is reasonable to use interpolation to determine productivity index as productivity index curves provided by the DVS method are linearly decreased with decreasing fracture conductivity in both transient and pseudo-steady state regimes.

TABLE 3.3—Modified inputs for calculation of productivity index in acid fracturing

Reservoir properties	xe, reservoir length, ft
	ye, reservoir width, ft
	ze, formation thickness, ft
	zgross, gross height, ft
	kx, permeability along the reservoir length direction, md
	ky, permeability along the reservoir width direction, md
	kz, permeability along the reservoir height direction, md
Source properties	c_x, x-coordinate of the center point of fracture
	c_y, y-coordinate of the center point of fracture
	c_z, z-coordinate of the center point of fracture
	w_x, fracture half-length, ft
	w_z, fracture half-height, ft
Acid properties	Vi, injected acid volume, bbl
	Vp, Volumetric dissolving power
	$\sigma_{h,\min}$, minimum horizontal stress, psi
	S_{rock}, rock embedment strength, psi
FBHP history	3 options available to input FBHP

Various productivity index curves are depicted in **Fig. 3.2**. In acid fracturing, fracture conductivity is obviously decreased with time since net closure stress acting on fracture wall increases as flowing bottomhole pressure decreases gradually to its minimum value, over the life of the well. Thus, if flowing bottomhole pressure history is specified, we can find the productivity index with the current value of dimensionless time using an interpolation function. The steps for creating an interpolation function and finding the productivity index using the interpolation function are described in **Tables 3.4** and **3.5**.

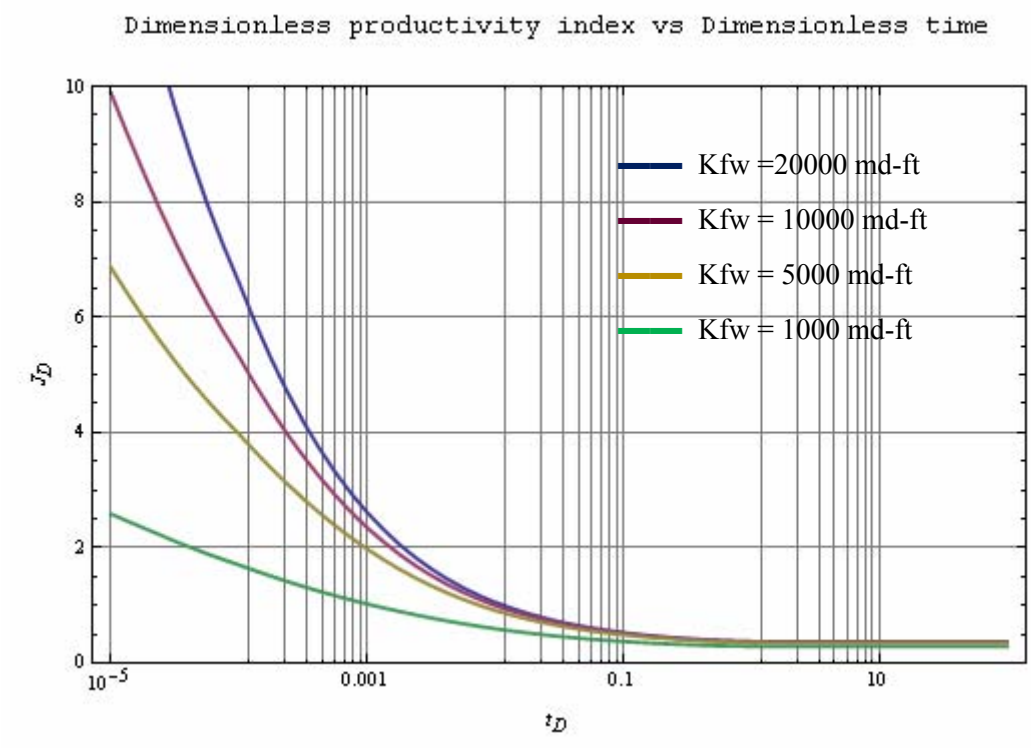

Fig. 3.2—Dimensionless productivity index curves with various acid fracture conductivity

TABLE 3.4—Steps to establish two variable interpolation function

1. Specify inputs such as reservoir properties and fracture properties

   reservbox: {xe, ye, ze, kx, ky, kz}

   sourcebox: {cx, cy, cz, wx, wy, wz, kfx}

2. Make interpolation points (11 points)

   conductivity range : 1*000md-ft to* 10^{11} *md-ft*

   e.g.) sourcebox1: {cx, cy, cz, wx, 0.05ft, wz, 10^12 md ft}

   sourcebox2: {cx, cy, cz, wx, 0.05ft, wz, 10^11 md ft}

   .

   .

   .

   .

   sourcebox11: {cx, cy, cz, wx, 0.05ft, wz, 10^4 md ft}

3. Calculate dimensionless productivity index with "calcJDfrac" function in DVS method for each interpolation point

   calcJDfrac[reservbox, sourcebox1…sourcebox11]

   In this step we can generate eleven dimensionless productivity index curve over dimensionless time

4. Make an two-variable interpolation function with eleven points data (using mathematica)

   Input values are acid fracture conductivity and dimensionless time (two variables)

   Inter2var[kfw, t_D] → J_D

   Output is dimensionless productivity index

TABLE 3.5—Steps to calculate J_D with two-variable interpolation function
1. Specify inputs such as reservoir properties and fracture properties reservbox:{xe, ye, ze, kx, ky, kz} sourcebox:{cx, cy, cz, wx, wy, wz, kfx}
2. Specify inputs such as acid properties and FHTP history acidinput:{Vi, VDP, Smin, Srock} FHTP:{Transpose[{time, flowing bottomhole pressure history}]} From these inputs, we can calculate acid fracture conductivity with Nierode-Kruk correlation (see Table 3.1) e.g.) AcidFracCond[pwf, reservbox, sourcebox, acidinput] → k_fw
3. Input acid fracture conductivity and dimensionless time to interpolation function * Dimensionless time is defined using the time when we specify flowing bottomhole pressure Inter2var[kfw, t_D] → J_D Output : dimensionless productivity index
4. Repeat 2-3 whenever FHTP and time change. In the end, we can obtain J_D vs t_D graph as same manner in DVS method.

3.3.1 Validation of Two Variable Interpolation Function

Using SA-1 well inputs, I validated the interpolation function with various acid fracture conductivity. An example of the validation is shown in **Figs. 3.6** and **3.7**. J_D obtained by DVS method is compared with J_D obtained by the two-variable interpolation function when acid fracture conductivity of both cases is 19822 md-ft. The interpolation function quite accurately determines J_D as the error between the DVS method and interpolation function, which remained within 4%.

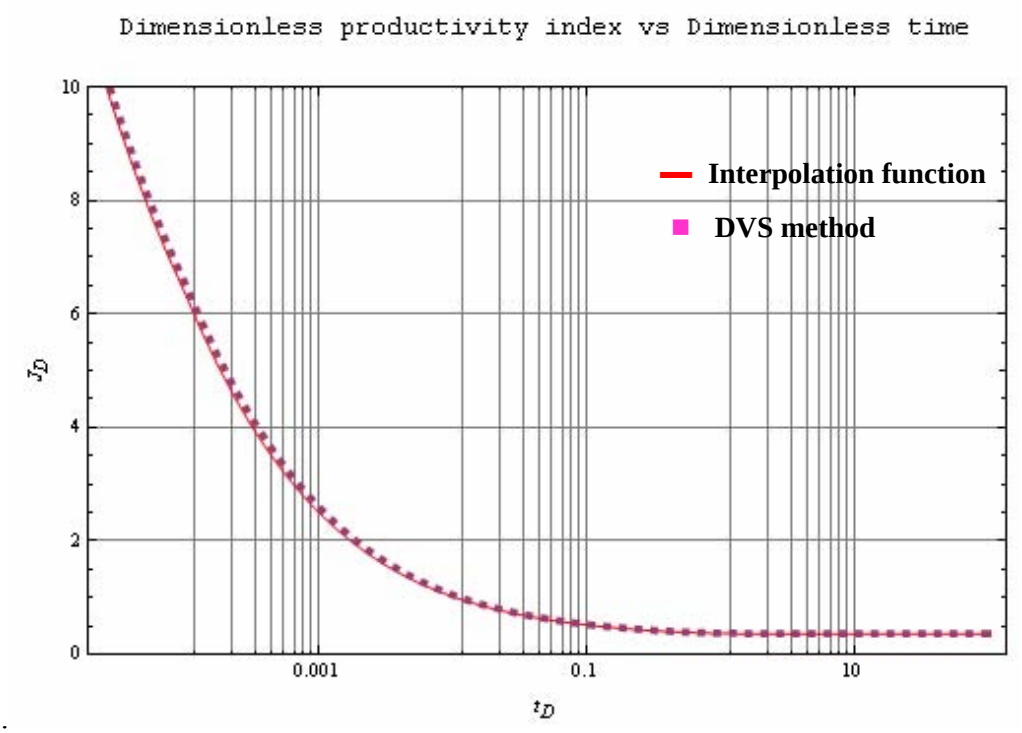

Fig. 3.3—Comparison of J_D from DVS method to J_D from interpolation function

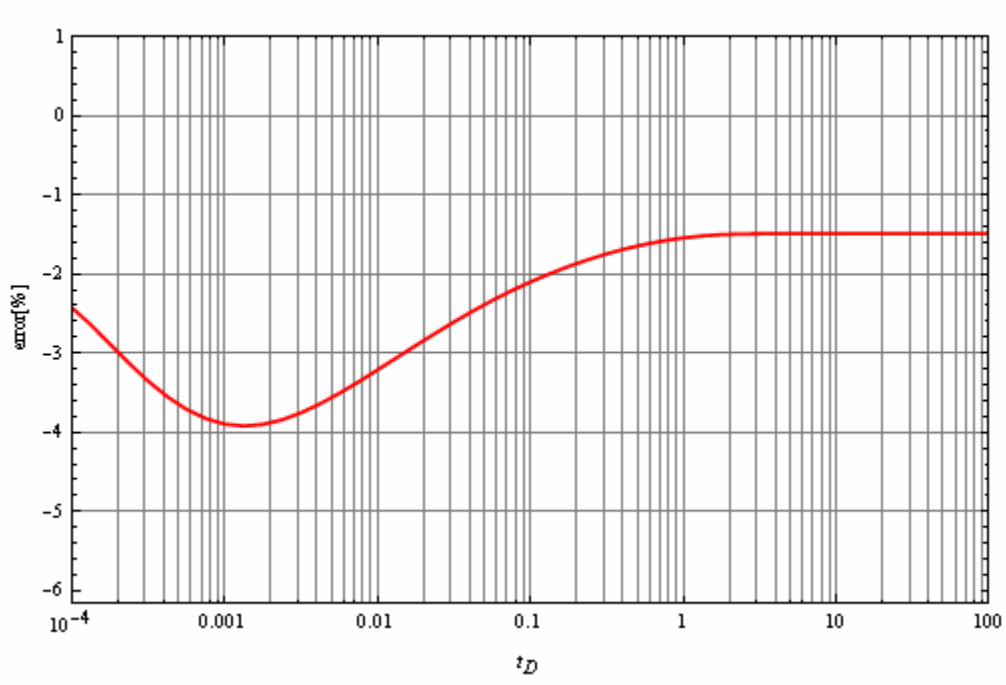

Fig. 3.4—Error in comparison of J_D from DVS method to J_D from interpolation function versus dimensionless time

3.3.2 Effectiveness of Two Variable Interpolation Method

In the previous section, I created a two-variable interpolation function to calculate J_D depending on variable acid fracture conductivity and dimensionless time. By using SA-1 well inputs, I will show the effectiveness of a two-variable interpolation method by comparing J_D determined by using constant fracture conductivity to J_D determined using a two-variable interpolation method. I use average acid fracture (=19,822 md-ft) conductivity of the SA-1 well as a constant fracture conductivity. Fracture conductivity of the SA-1 well is calculated by the Nierode-Kruk correlation based on SA-1 well FBHP history, ranging from 8816.9 md-ft to 28606.7 md-ft. **Fig. 3.5** illustrates changes in JD over dimensionless time for the two different cases: JD calculated with constant conductivity, and JD determined with the interpolation method. The difference between the two cases is very small most of the time, as shown in **Fig. 3.6**.

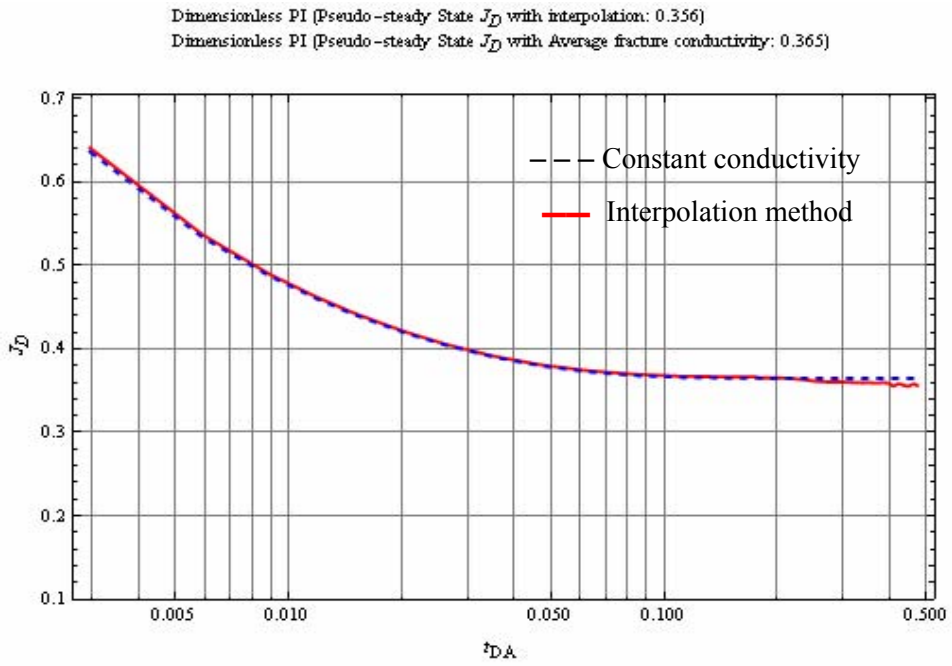

Fig. 3.5—Comparison of J_D using interpolation method to J_D using constant conductivity versus dimensionless time

As shown in both **Fig. 3.5 and 3.6**, there was no distinguishable difference between two different cases, especially at the beginning. The discrepancy becomes greater as conductivity is less than 10,000 md-ft. The error remains within 2.5% when acid fracture conductivity is greater than 10,000 md-ft as shown in **Fig. 3.7**. Therefore, it is reasonable to use average fracture conductivity for a case having more than 10,000 md-ft of conductivity.

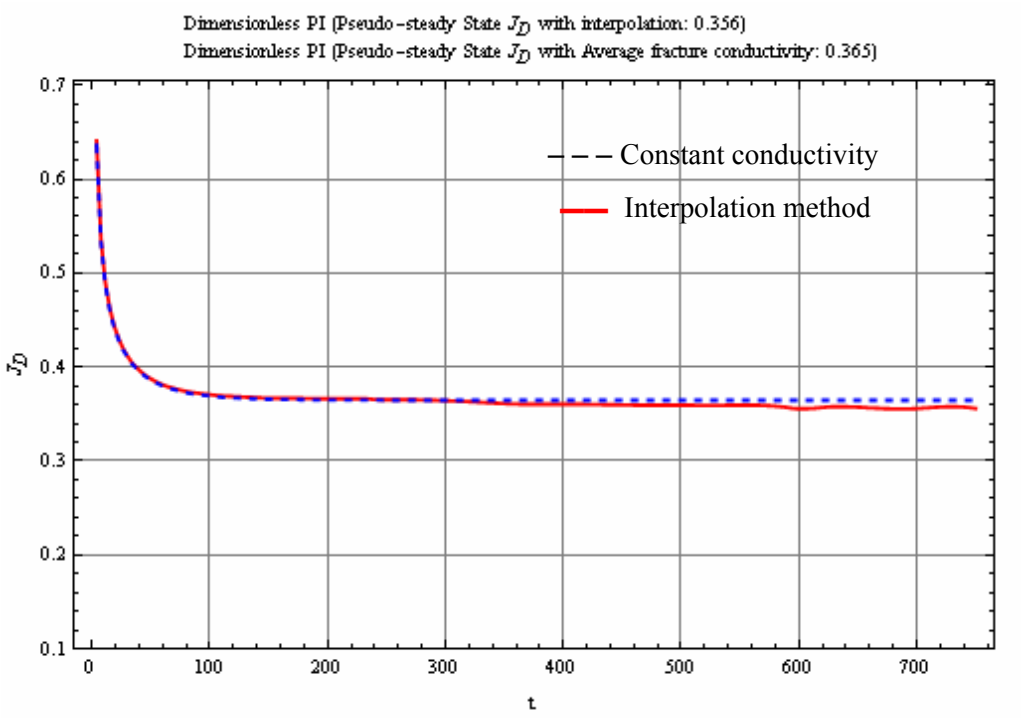

Fig. 3.6— Comparison of J_D using interpolation method to J_D using constant conductivity versus time

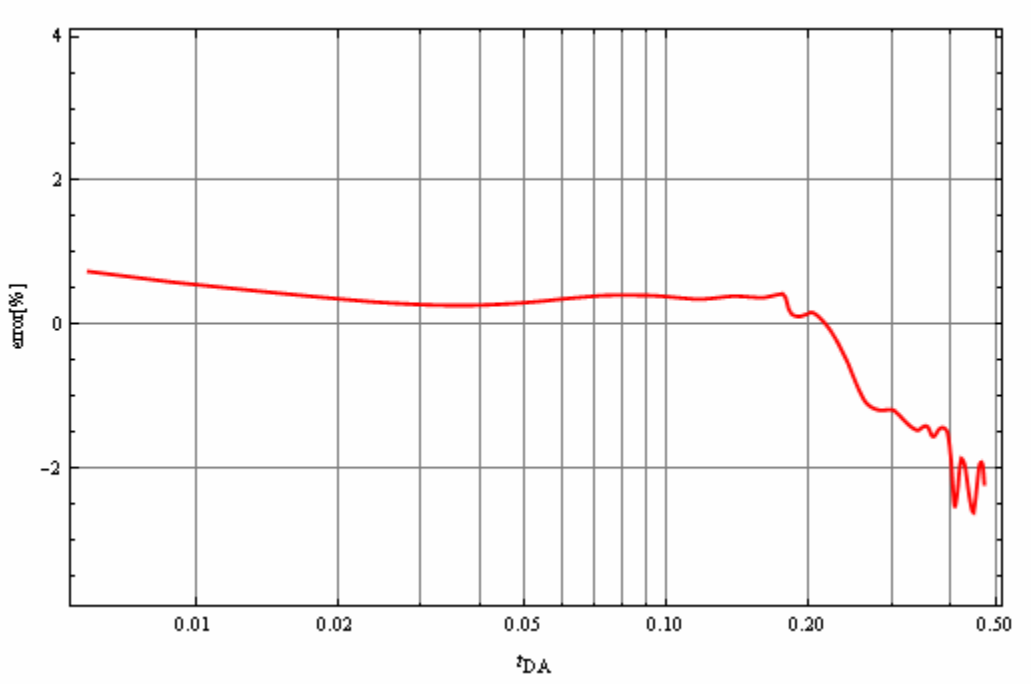

Fig. 3.7— Error analysis in comparison of J_D using interpolation method to J_D using constant conductivity.

Well SA-1 had produced gas for only two years and this is a relatively short lifetime to detect JD change when fracture conductivity is lower than 10000 md-ft. To compensate for the short term of well history in detecting changes in J_D, I ran a simulation for a case with the same inputs used in SA-1, but with different FBHP history. FBHP decreases from 6783 psi to 3833 psi for a 60-month production period and fracture conductivity varies from 28606.7 to 6300 md-ft.

Fig. 3.8 and **Fig. 3.9** show discrepancies between J_D using the interpolation method and J_D using constant conductivity case, and the differences increase. The percentage of discrepancy is up to 4%, as shown in **Fig. 3.10**. As a reservoir is depleted, the bottomhole pressure of the well decreases and fracture conductivity deteriorates. In

this case, the interpolation method provides more accurate J_D than does the constant conductivity method.

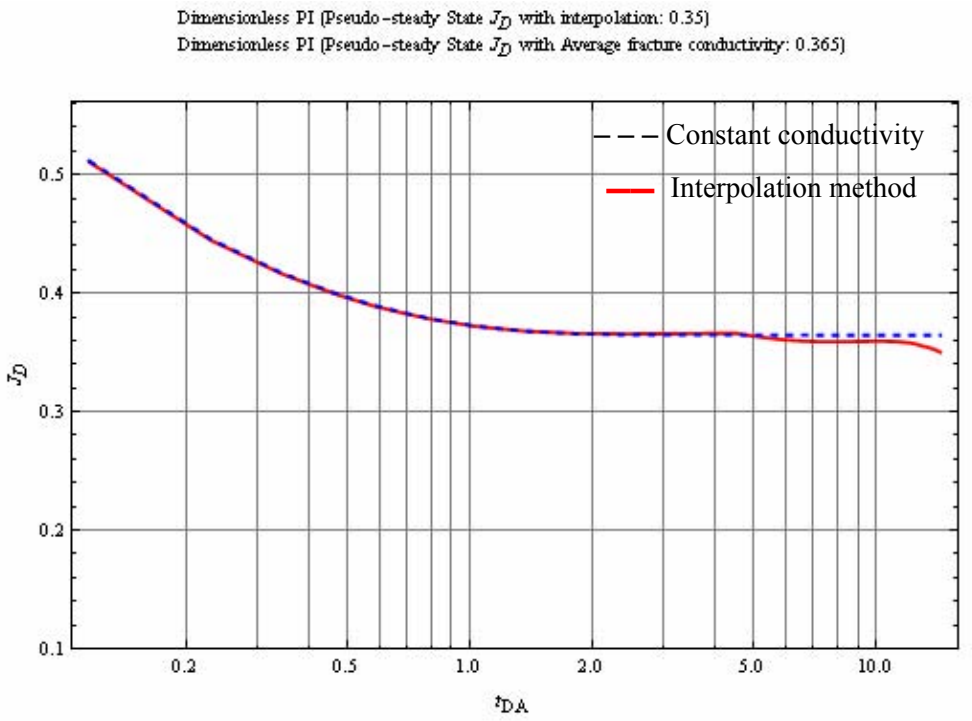

Fig. 3.8—Comparison of J_D using interpolation method to J_D using constant conductivity versus dimensionless time (60 months production).

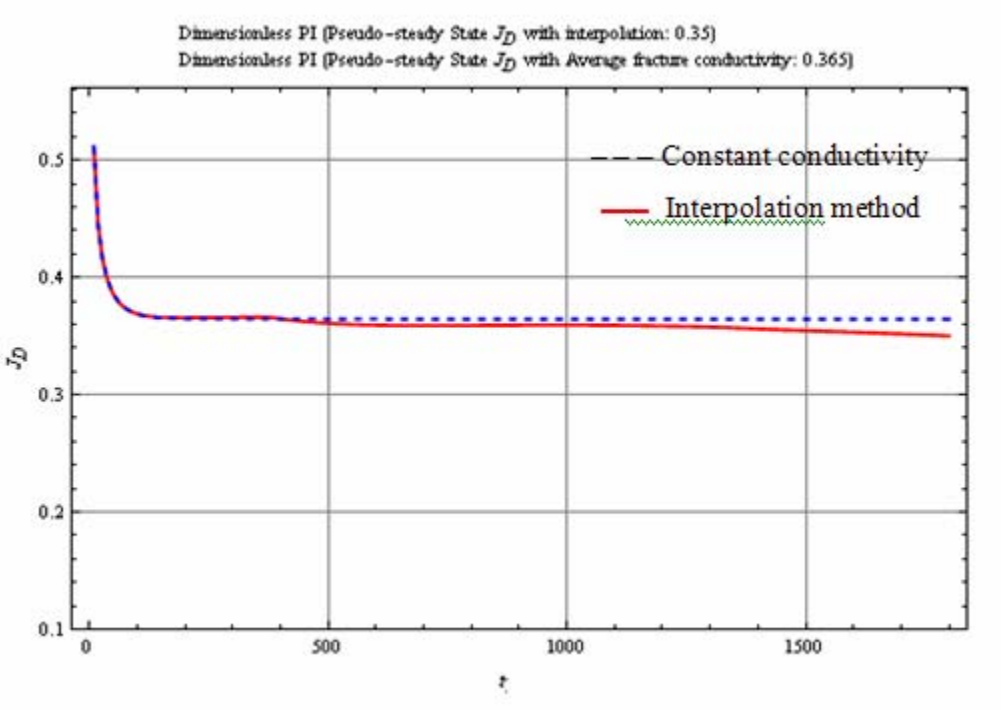

Fig. 3.9—Comparison of J_D using interpolation method to J_D using constant conductivity versus time (60 months production).

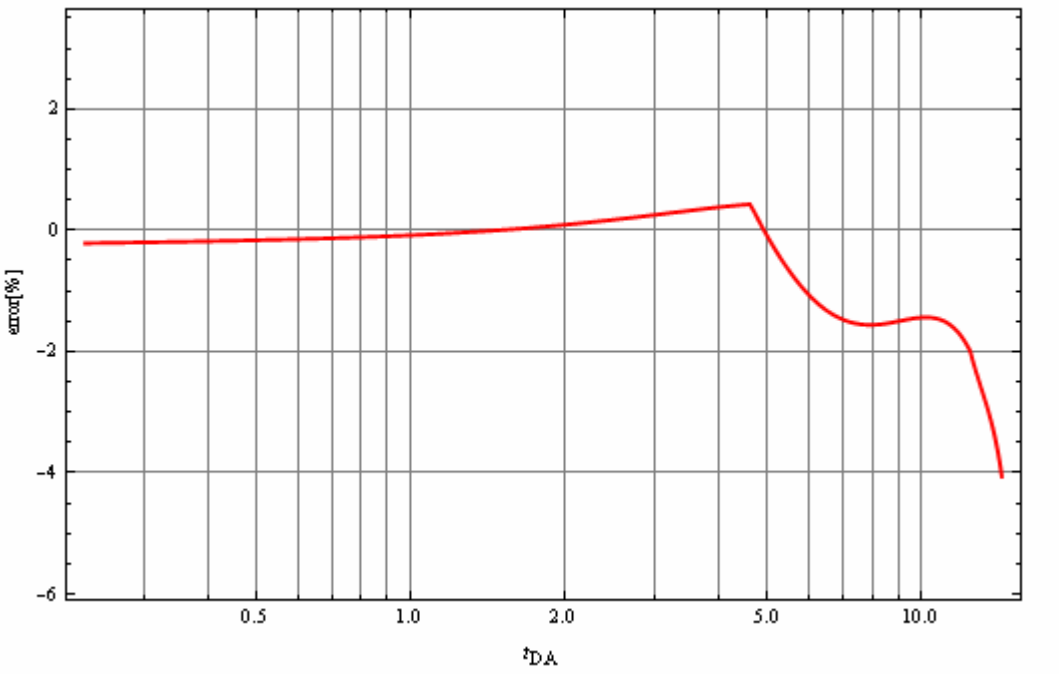

Fig. 3.10— Error analysis in comparison of J_D using interpolation method to J_D using constant conductivity (60 months production).

3.4 The Effect of Fracture Shape

In DVS method, the source, in other words, the fracture, is described as a box-volumetric source inside of the rectilinear shaped reservoir. But in reality, fracture shape is closer to elliptical, so we need to investigate the effect according to fracture shape. **Figs. 3.11** and **3.12** show diagrams of a rectangular fracture and an elliptical fracture.

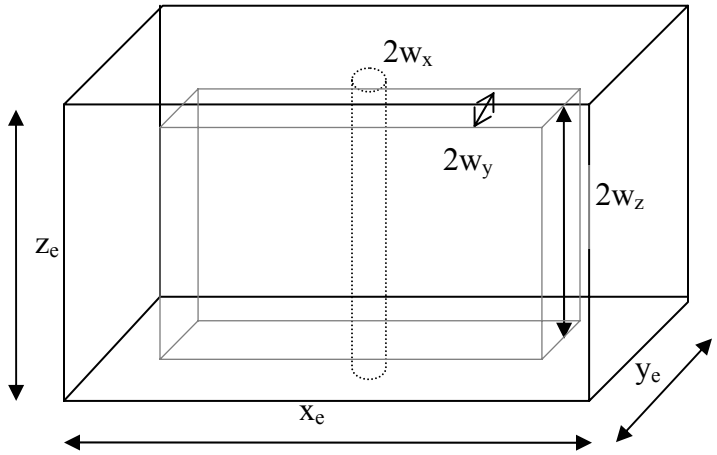

Fig. 3.11—A vertical well with rectangular fracture

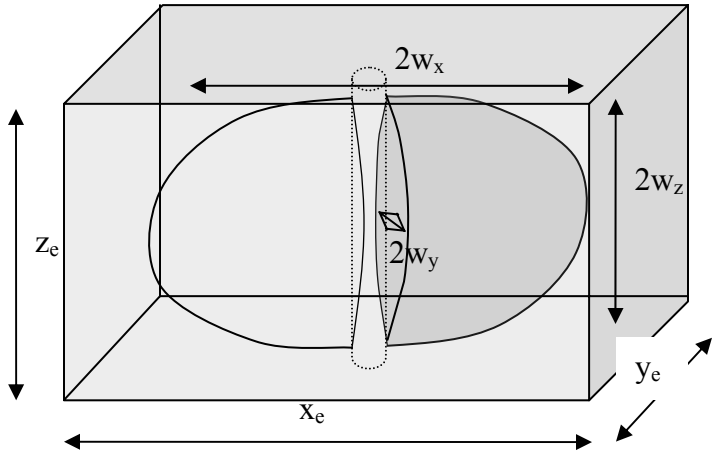

Fig. 3.12—A vertical well with elliptical fracture

Fortunately, this kind of research has been conducted by Jin (2008) in a proppant fracturing case. In his research, linear distribution function for fracture width, height and proppant pack permeability was defined using the equivalent proppant volume. I incorporated width and height interpolation functions, which were introduced in Jin's dissertation, into my program. Basically, we cannot define fracture width and fracture permeability in the acid fracturing case, so I use ideal width in the Nierode-Kruk correlation as a basic input for making a various width profile. Therefore various fracture permeability is determined by dividing fracture conductivity by various width. Strictly speaking, a various width profile and various fracture permeability do not really affect pressure response of the reservoir because the product of width and permeability is equal to acid fracture conductivity itself, which was obtained from the Nierode-Kruk correlation. We can use fracture height in our input data for the various height profile and various fracture height will affect the pressure response and the dimensionless productivity index. The results of simulations with rectangular fracture and elliptical fracture are shown in **Fig. 3.13.**

I use input data from the SA-1 well. In both transient regime and pseudosteady-state regime, J_D in the elliptical fracture is slightly bigger than J_D in the rectangular fracture. In this case, the discrepancy is small enough to negligible, so we can use either elliptical fracture or rectangular fracture in acid fracturing. By using both fracture shapes, we can investigate the effects of fracture shape. **Fig. 3.14** shows us the elliptical fracture shape in the program.

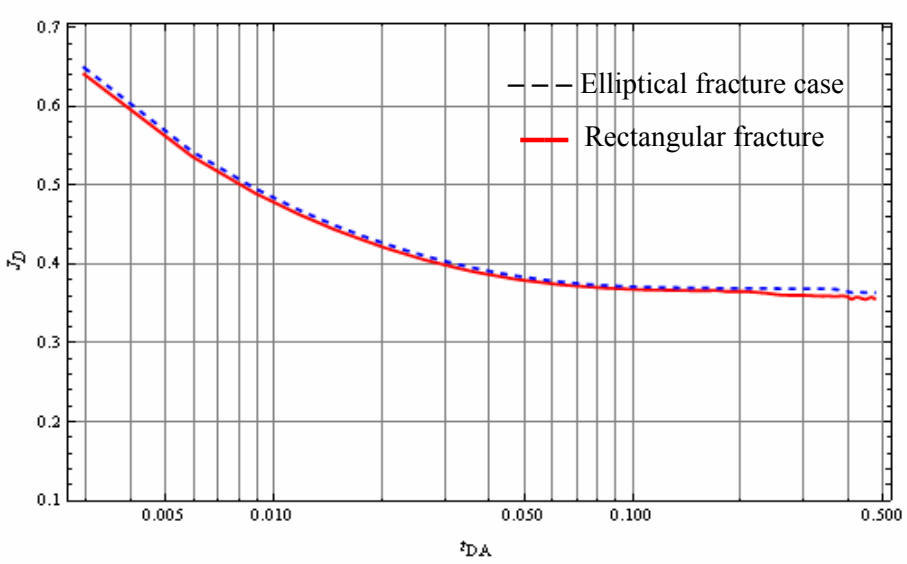

Fig. 3.13—Comparison of J_D in rectangular fracture to J_D in elliptical fracture versus dimensionless time.

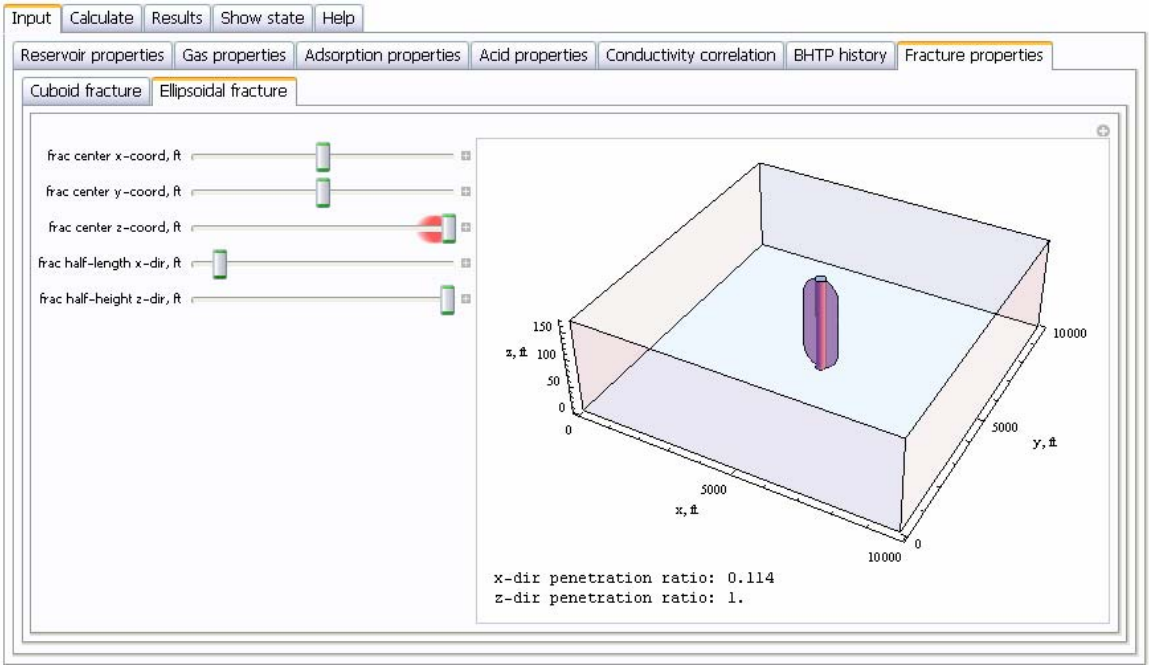

Fig. 3.14—A model of elliptical fracture in “Gas Acid” program.

3.5 Production Forecasting

To forecast production, we combine the productivity index with material balance. Material balance relates the produced gas with the reservoir pressure depletion giving us the important information about average reservoir pressure. To calculate the average reservoir pressure in a gas reservoir, only expansion of fluid needs to be considered. Assuming isothermal operation the average pressure equation can be given as

$$\bar{p} = \frac{p_i Z}{Z_i}\left(1 - \frac{G_p}{G_i}\right) \quad \text{(2.21)}$$

Where G_p is the cumulative production and G_i is the initial gas in place.

The pseudo-steady state solution of radial flow of compressible fluid can be solved as following, if the original diffusivity equation is derived in terms of real gas pseudopressure of Al-Hussainy and Ramey (1965)

$$q_{sc} = \frac{\sqrt{k_x k_y}\,h}{1424T} \times J_D \times \left[m(\bar{p}) - m(p_{wf})\right] \quad \text{(2.21)}$$

Where a real gas pseudopressure function, m(p), is defined in **Table 3.6**. The notation J_D indicates that we should use the dimensionless productivity index corresponding to the dimensionless equivalent of the current time (elapsed from the start of the production).

To describe the part of the production during the transient period as well, we need a description of J_D covering the whole time span (Economides *et al*., 2007). Strictly speaking, such a complete presentation is possible only for well defined flow history. Mathematically, the easiest method is to handle the constant-rate type flow history. In such case, the late-time stabilized part is called pseudo-steady state. Other types of flow histories, e.g. the one implicitly defined by constant wellbore pressure, may lead to slightly different productivity indices at any moment of time and even their stabilized

value might differ from the pseudo-steady state one according to Helmy and Wattenbarger (1998).

Of course it is possible to calculate a productivity index curve for any specified rate history but that would be unpractical in general. In reality, we cannot know ahead the production history that would happen in future of the fractured well. Fortunately, the productivity index curve with constant-rate condition is generally a good average indicator and any particular production history can be forecast with reasonable accuracy with it. We can use the results of DVS method to generate the combined J_D curve that describes both the transient and the stabilized (pseudo-steady state) production regime (Economides *et al*., 2006).

A rather straightforward approach to forecast the production from a fractured well is depicted in **TABLE 3.6**. For gas reservoirs, gas properties changes as reservoir pressure changes, so the properties need to be redefined when reservoir pressure changes over the time. To define dimensionless time, we use current time for t (elapsed time from the start of the production) and use one time step before current time pressure to calculate μ and c_t which are functions of pressure. Viscosity and total compressibility of the previous time step are assumed to be same as those of current time since we use quite small time steps and pressure differences between two time steps are small enough to be negligible.

TABLE 3.6—Production forecast method (Field units)

1. Prepare gas functions for z-factor, compressibility and viscosity using correlation (details are in Appendix A)

2. Prepare pseudopressure function

$$m(p) = 2\int_{p_0}^{p} \frac{p'}{(\mu Z)_{p'}} dp'$$

3. Specify initial pressure p_i

4. Specify wellbore flowing pressure p_{wf} in current time (initially $t = \Delta t$)

5. Calculate acid fracture conductivity with p_{wf} using Niroede-Kruk correlation

6. Calculate gas properties with reservoir pressure (compressibility and viscosity are function of pressure)

7. Define dimensionless time with current time and gas properties

$$t_D = \frac{k}{\phi \mu c_t L^2} t \quad \text{where } k = (k_x k_y k_z)^{\frac{1}{3}},\ L = (x_e y_e z_e)^{\frac{1}{3}}$$

8. Using two-variable interpolation function with acid fracture conductivity and dimensionless time, specify J_D at current time

Inter2var[kfw, t_D] → J_D

9. Take a time interval Δt

10. Calculate production rate and production in the time interval

$$q_{sc} = \frac{\sqrt{k_x k_y}\, h}{1424\, T} \times J_{D,t_D} \times \left[m(\bar{p}) - m(p_{wf})\right] \quad \text{and} \quad \Delta G_p = q_{sc} \Delta t$$

11. Apply material balance and calculate new average pressure

$$\bar{p} = \frac{p_i Z}{Z_i}\left(1 - \frac{G_p}{G_i}\right)$$

12. Current time, $t = t + \Delta t$

13. Repeat steps 4-12.

3.6 Optimization of Fracture Half Length

As stated earlier, "Gas Acid" can be a useful tool, suitable for inferring created fracture parameters. In acid fracturing, the important factors controlling the effectiveness of acid fracturing are fracture half length and fracture conductivity. It is impossible to estimate fracture width in acid fracturing, so optimum fracture dimension means optimum fracture half length with given fracture height and fracture conductivity. If we run the program with various fracture half lengths and other inputs remain unchanged, optimum fracture half length can be obtained in view of maximum production. An example run of the SA-1 well case is shown in **Fig. 3.15** and optimization data is available in **Table 3.7**.

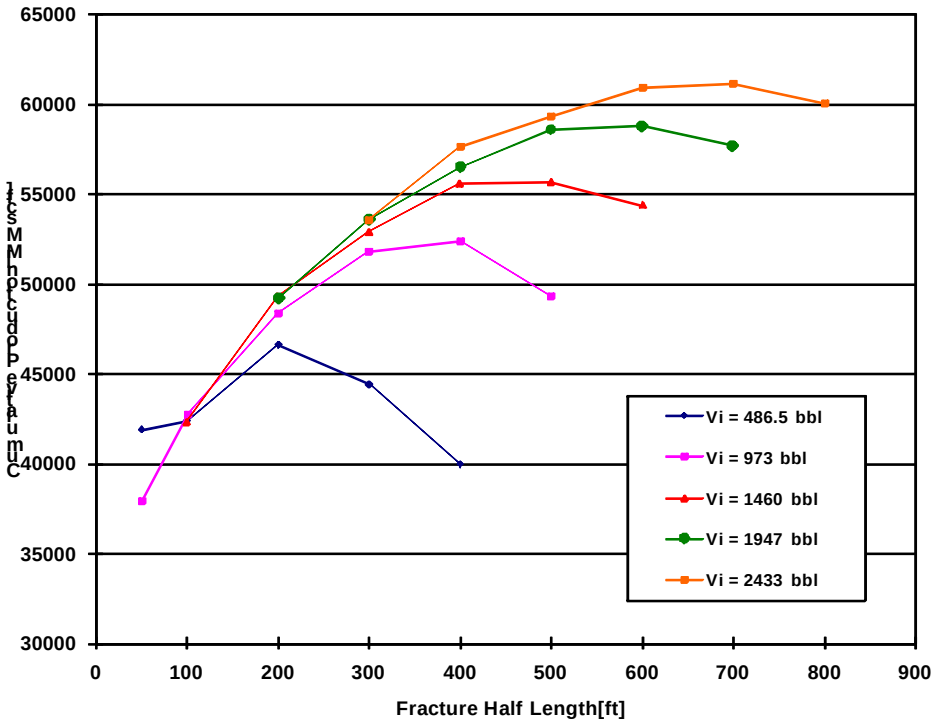

Fig. 3.15—Fracture half length versus cumulative production with various acid volumes

If we use optimum fracture half length in simulation, more acid volume results in more cumulative production (see **Fig. 3.16**). However, we must consider the economic efficiency of acid volume because if a larger amount of acid volume is used and the amount of stimulated production is not considerable, then we do not need to use more acid volume. If the gas price is high, then we may try to recover more gas, regardless of acid volume and cost. But if gas price is low, we may have to consider economic efficiency in acid volume. By considering the prices of both acid and gas and using the program, we might find the optimum acid volume for the well.

Table 3.7 – Optimization data from SA-1

Injected Acid Volume [bbl]	Fracture Half Length [ft]	Cumulative Production [MMSCF]
486.5	205.512	46600
973	356.7	52164.3
1460	450.459	55900
1947	556.732	58912.6
2433	658.711	61300
2920	753.189	63200

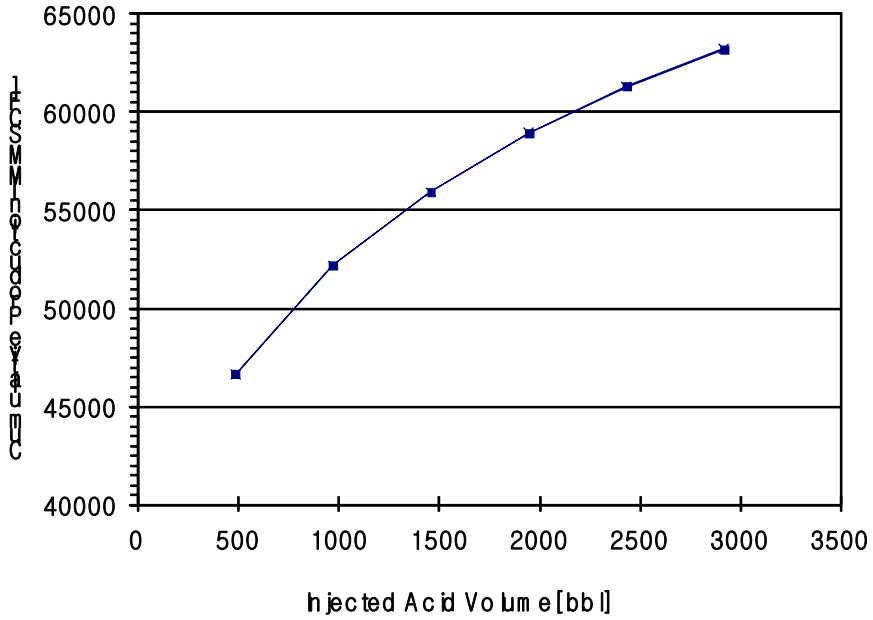

Fig. 3.16—Injected acid volume versus cumulative production with optimum fracture half length

CHAPTER IV

FIELD CASES

4.1 Reservoir Description

The Khuff formation is a deep gas carbonate reservoir that consists of dolomite and limestone sections underlying the giant Ghawar oil field in the eastern region of Saudi Arabia (Bartko *et al*., 2003). The Khuff formation is ideal for acid fracturing because of the heterogeneous nature of the formation, which tends to support the created fracture conductivity. The Khuff and pre-Khuff are deep gas condensate reservoirs in an active tectonic stress environment (Al-Qahtani, 2001). This formation belongs to the late Permian age and lies between 11,000 and 12,000 ft. The Khuff formation is subdivided into four main zones, denoted as A, B, C, and D, and the two main producing zones are Khuff B and Khuff C. Both reservoirs have been tested and proven to have a high quantity of condensate rich gas. The average pay thickness in each reservoir is estimated to be 110 ft and 180 ft for Khuff B and Khuff C, respectively (Rahim *et al*., 2001). The acid fracturing field data used in this study was originally provided by Saudi Aramco Oil Company. Previously, Alghamdi (2005) used adjusted raw data and calculated value such as fracture half length, and FBHP using simulation programs. I use the adjusted data set from his dissertation. However, I reproduced FBHP history using PROSPER.

4.2 Field Applications

Two field cases from Saudi Aramco, where acid fracturing treatments have been performed, were used to validate the "Gas Acid" program. Reservoir characteristics, the fracture geometry and acid properties will be described and used as inputs for the program.

4.2.1 Well Description

Acid fracture treatment data have been provided on wells SA-1, SA-2. The treated zone is Khuff-C for SA-1 and SA-2. In this chapter, we use SA-1 and SA-2 data and show the results.

SA-1 : Acid fracturing treatment of SA-1 well was performed in the Khuff C zone. There are two sets of perforations in the SA-1 well. The upper Khuff-C which is between 11,402 and 11,525 ft was perforated with 6 shots per foot. The lower Khuff-C from 11,525 to 11,575 ft was perforated with 1 shot per foot. Permeability of the producing zones is from 1.22 to 4.0 md and porosity varies from 7.5 to 20%. We use arithmetic average permeability of 2.21md and arithmetic average porosity of 11.5 % as input data. The reservoir data are summarized in **Table 4.1**. The reservoir temperature was estimated to be 270ºF. A net pay of this well is 151 ft. The mechanical properties of the rock include a Poisson ratio of 0.29, and a Young's modulus of 6.1E+6 psi. The average in-situ stress is 10,400 psi and average reservoir pressure is 7,500 psi. The well has a gas with specific gravity of 0.79 and a drainage area of 2250 acres. Embedment strength is measured in the laboratory and ranges between 30,000 psi to over 100,000 psi in the Khuff formation (Nasr-El-Din *et al*., 2002). I used 100,000 psi as an average value of the embedment stress. Average reservoir data and other well characterization data are summarized in **Table 4.2**.

TABLE 4.1—SA-1 reservoir data							
Layer	Start of Interval	End of Interval	Thickness of interval	Permeability (md)	Porosity (%)	Kh, (md-ft)	Sg (%)
1	11,402	11,425	23	1.22	8	28.06	70
2	11,440	11,452	12	1.50	12	18.00	85
3	11,458	11,500	42	1.44	10	60.48	85
4	11,501	11,525	24	1.18	7.5	28.32	40
5	11,525	11,575	50	4.0	20	200.0	88

TABLE 4.2—SA-1 average reservoir data and well characterization			
Parameter	Value	Parameter	Value
Net pay	151.0 ft	Reservoir Temperature	270.0 oF
Permeability	2.22 md	Gas specific gravity	0.79
Growth thickness	173 ft	Reservoir pressure	7500 psi
Average porosity	11.5 %	Drainage area	2250 acre
Average gas saturation	73.6 %	In-Situ Stress	10,400 psi
Viscosity	0.035 cp	Rock embedment strength	100,000 psi

As seen in **Table 4.3**, the volumes of acid pumped into well SA-1 for each stage are presented. From these data, total acid volume is calculated and I use 81,800 gal (=1947.6 bbl) as acid volume, which is an input value for the Nierode-Kruk correlation used to estimate acid fracture conductivity.

TABLE 4.3—SA-1 pumping schedule				
Stage Name	Slurry Rate (bbl/minute)	Pump Time (Minute)	Slurry Volume (bbl)	Acid Volume (gal)
Pad (polymer gel)/ Acid	48.5	9.3	451	16,879
Pad (polymer gel)/ Acid	58.4	7.4	432	16,172
Pad (VES)/ Acid	64.6	6.6	426	15,955
Pad (VES)/ Acid	67.4	8.9	599	22,447
Closed Fracture Acid	55.3	5	276	10,347

Because field data for fracture geometry are not available, I simply use the fracture geometry that was predicted before the fracturing treatment using the design model (fracCADE) provided by the service company. Thus, the fracture half length is assumed to be the design value and I use 378.9 ft for the SA-1 well.

SA-2: The SA-2 well was drilled to 11,377 ft depth and is also completed in the Khuff-C zone. Reservoir data and well characterization are summarized in Tables 4.4 and 4.5. Also, the pumping schedule for the acid stages is given in Table 4.6. Total acid volume is 1662.58 bbl and designed fracture half length is 413 ft.

TABLE 4.4—SA-2 reservoir data

Layer	Start of Interval	End of Interval	Thickness of interval	Permeability (md)	Porosity (%)	Kh (md-ft)	Sg (%)
1	11,377	11,387	10	3.49	17	34.9	85
2	11,389	11,398	9	1.28	10	11.52	78
3	11,400	11,430	30	0.84	8	25.2	76
4	11,460	11,470	10	3.88	18	38.8	80
5	11,502	11,532	30	0.49	6	14.7	75

TABLE 4.5—SA-2 average reservoir data and well characterization

Parameter	Value	Parameter	Value
Net pay	89 ft	Reservoir Temperature	250 ^{o}F
Permeability	1.4 md	Gas specific gravity	0.79
Growth thickness	155 ft	Reservoir pressure	7,505 psi
Average porosity	11.8 %	Drainage area	2250 acre
Average gas saturation	78.8 %	In-Situ Stress	10,830 psi
Viscosity	0.035 cp	Rock embedment strength	100,000 psi

TABLE 4.6—SA-2 pumping schedule				
Stage Name	Slurry Rate (bbl/minute)	Pump Time (Minute)	Slurry Volume (bbl)	Acid Volume (gal)
Pad (polymer gel)/ Acid	38.9	9.8	381	11,207
Pad (polymer gel)/ Acid	45.8	8.3	380	11,176
Pad (VES)/ Acid	51.9	8.1	420	16,491
Pad (VES)/ Acid	51.7	8.3	429	16,833
Closed Fracture Acid	23.7	14.3	338	14,120

4.2.2 Production History and FBHP Calculation

Production history of wells SA-1 and SA-2 for two years was provided by Saudi Aramco and used to match the simulation results for PI, production rate and cumulative production. A couple of daily production reports and PVT data collected in the field development stage were sufficient to build models for two wells (SA-1, SA-2) in PROSPER, a nodal analysis software. **Tables 4.7** and **4.8** show reservoir properties used in simulation. Each well was perforated for several zones and this multi-zone perforation was simplified in the simulation by adding thickness of all intervals for each well. Permeability and porosity values are different for each zone and the average values were used as valid measures in the simulation program.

Table 4.7—Reservoir properties input in nodal analysis					
Well Name	Res. Initial Pressure (psi)	Res. Temp (°F)	Net Pay (ft)	K (md)	Φ (%)
SA-1	7500	270	151	2.22	12.8
SA-2	7555	259	89	1.41	9.7

I have assumed Condensate Gas Ratio (CGR or condensate yield) is constant for 2-year production period as no condensate production data was consistently reported for this field.

Table 4.8—PVT data input in nodal analysis

Well Name	Gas gravity (fraction)	Condensate gravity (°API)	Condensate gas ratio (STB/MMSCF)	H_2S (mole%)	CO_2 (mole%)	N_2 (mole%)
SA-1	0.79	46.2	70	0.9	1.53	8.5
SA-2	0.79	53	89	N/A	0.57	7

Due to lack of Bottom Hole Pressure (BHP) data during production, no flowing tubing correlation match was achieved, so a tubing integrity check was not possible. Therefore, to calculate Flowing Bottom Hole pressure (FBHP), production rates (gas, water, and condensate) were used with Petroleum Experts Flow Tubing Correlation which is implemented in Prosper. Since only initial reservoir pressure is known and no static pressure survey data exists, average reservoir pressure needed to be estimated to match production history. VLP and IPR curve matching was done for the first month of production, as shown in **Fig. 4.1**.

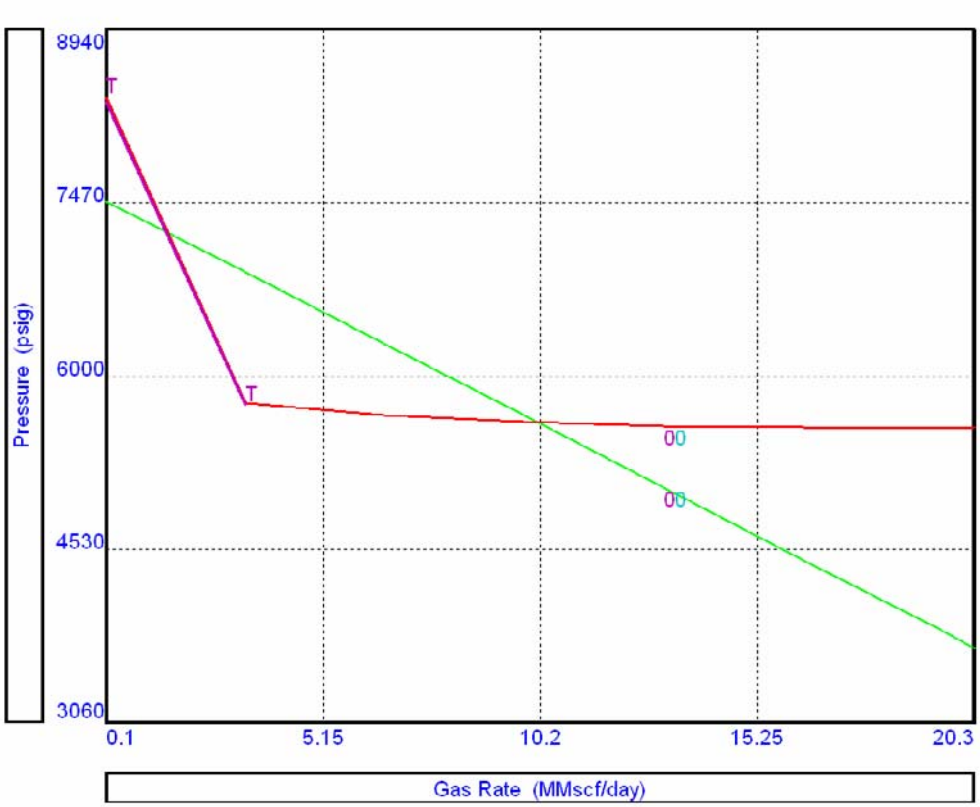

Fig. 4.1 – For Well SA-2, IPR and VLP curves show production rates at the beginning of production.

I have applied different reservoir pressures for IPR & VLP curves, and about 400-500 psi reservoir pressure drop was estimated with an educated guess over the 2-year production period, as shown in **Fig. 4.2**. This may result in the average reservoir pressure having less accuracy, but the errors should fall within an acceptable range, as possible maximum reservoir pressure drop is only about 1,500 psi to keep a well producing based on VLP curve, which is calculated using PVT data and well configurations. The evolution of reservoir pressure during production was assumed to be linear to time since cumulative productions over whole time period for all wells were linear to time. Once average reservoir pressure was estimated, skin values were calculated in Prosper to corresponding reservoir pressure and production rates. A dimensionless productivity

index (Jd) was determined for each skin value and this dimensionless PI was used to match the results from Gas Acid. Data analysis for each well is given in Appendix D.

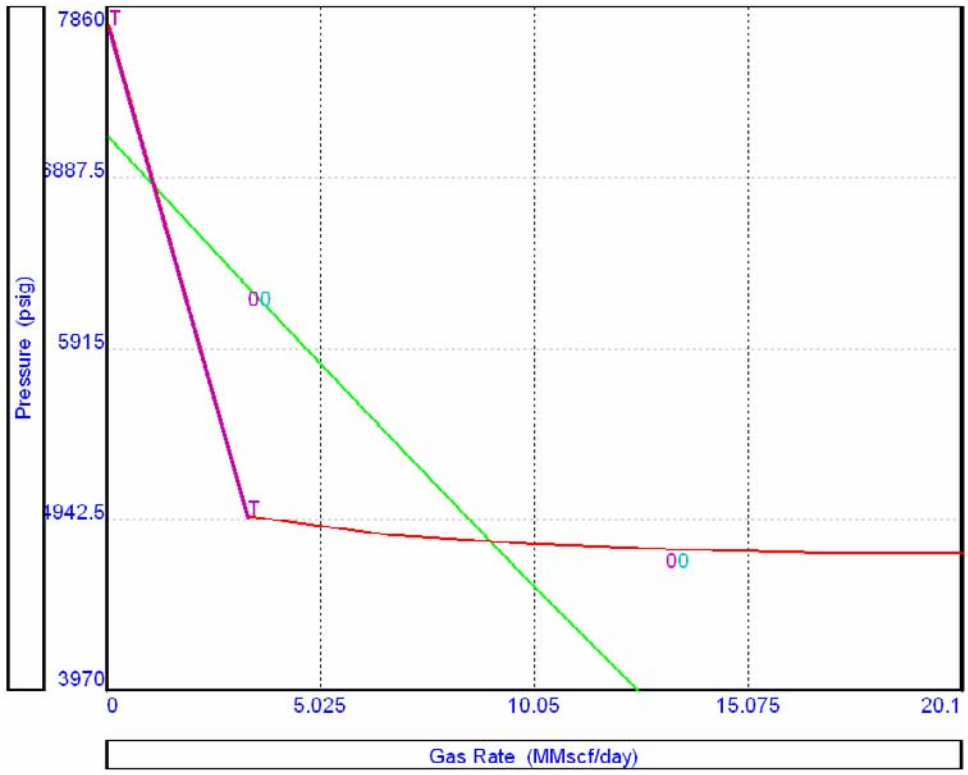

Fig. 4.2 – For Well SA-2, IPR & VLP curves show production rates at the end of production history; the absolute open flow (AOF) of IPR is much less after 2-year production.

4.2.3 Input Data Summary

Input data for simulation work using Gas Acid is described in **Tables 4.9** and **4.10**. FHTP data is one piece of important input data in the Gas Acid program (see Appendix D for FHTP data).

Table 4.9-Input data for SA-1

Reservoir geometry			Reservoir properties			Gas properties			Fracture geometry			Acid Inputs		
parameter	value	unit	parameter	value	unit	parameter	value	unit	parameter	value	unit	parameter	value	unit
xe	9842	ft	porosity	0.115	-	gas gravity	0.79	-	cx	4921	ft	acid volume	1947.6	bbl
ye	9842	ft	water saturation	0.21	-	N_2 molefraction	0.085	-	cy	4921	ft	volumetric dissolving power	0.178	-
ze	151	ft	Initial pressure	7500	psi	CO_2 molefraction	0.0153	-	cz	75.5	ft	gross height	173	ft
kx	2.22	md	rock Compressibility	1.355 x E(-5)	1/psi	H_2S molefraction	0.009	-	wx	378.8	ft	fracture half length	378.8	ft
ky	2.22	md	water compressibility	1.355 x E(-5)	1/psi	temperature	270	ºF	wz	75.5	ft	minimum horizontal stress	10400	psi
kz	2.22	md	-	-	-	-	-	-	-	-	-	Rock embedment stress	100000	psi

Table 4.10-Input data for SA-2

Reservoir geometry			Reservoir properties			Gas properties			Fracture Geometry			Acid Inputs		
parameter	value	unit	parameter	value	unit	parameter	value	unit	parameter	value	unit	parameter	value	unit
xe	9842	ft	porosity	0.118	-	gas gravity	0.79	-	cx	4921	ft	acid volume	1662.58	bbl
ye	9842	ft	water saturation	0.21	-	N_2 molefraction	0.07	-	cy	4921	ft	volumetric dissolving power	0.161	-
ze	89	ft	Initial pressure	7505	psi	CO_2 molefraction	0.0051	-	cz	44.5	ft	gross height	155	ft
kx	1.4	md	rock Compressibility	1.355 x E(-5)	1/psi	H_2S molefraction	10^(-7)	-	wx	413.8	ft	fracture half length	413	ft
ky	1.4	md	water compressibility	1.355 x E(-5)	1/psi	temperature	250	ºF	wz	44.5	ft	minimum horizontal stress	10400	psi
kz	1.4	md	-	-	-	maximum pressure	7505	psi	-	-	-	Rock embedment stress	100000	psi

4.2.4 Simulation Results

In this section, I will demonstrate the comparison results between simulation data using the "Gas Acid" program and field data, in terms of the dimensionless productivity index, production rate and cumulative production. As noted in the previous section, the field dimensionless productivity index was calculated by nodal analysis and those values were compared with simulation results. Production rate and cumulative production were directly taken from production data in the field. However, both SA-1 and SA-2 are wet gas wells and "Gas Acid" is programmed for a dry gas well, so the field data was adjusted. I converted condensate amount to gas using API, CGR and gas specific gravity and added the condensate amount as a gas to the field production data. History matching of the production is the most important factor for evaluating the program, and calculating the productivity index is one of the main analyses used to describe the performance of the well and evaluate the program.

SA-1: **Fig. 4.3** shows different dimensionless productivity indices between field data and Gas Acid simulations. In field data, we see a transient state regime from 1st to 9th month and a productivity index range between 0.11 and 0.47. But in simulation results, the transient regime is finished in 3-4th month and the productivity index decreases from 0.64 to 0.36. Until the 17th month, the J_D value discrepancy between field and simulation data is within 25-30%. Especially from the 11th to 17th months, the J_D of both cases are well matched because J_D in the field data become stable, like the pseudo-steady state regime. However, after the 17th month, we can find a sudden drop of J_D in the field and the drop results in a more than 40% reduction in J_D. I will address this sudden drop of J_D more specifically in the next chapter.

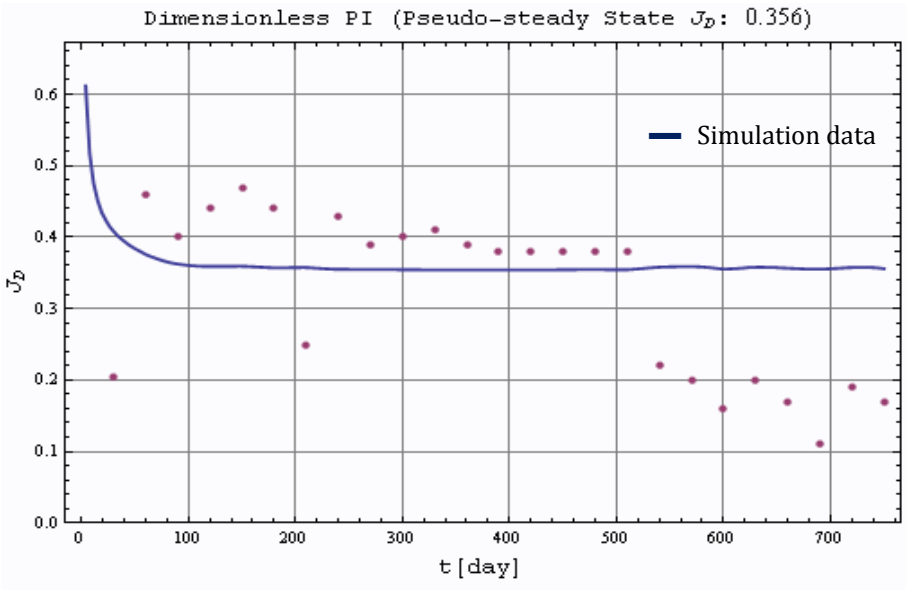

Fig. 4.3—Dimensionless productivity index versus time for well SA-1

In Gas acid simulation, **Fig. 4.4** shows a sudden increase in gas production after the 17th month of production, as FBHP was decreased, but J_D was stabilized. Well SA-1,

however, had no increase in production with higher DrawDown (DD). Comparing **Fig. 4.3** to **Fig. 4.4** allows us to detect problems on the well even though the well produces constant gas rates. From PVT data, Condensate Gas Ratio (CGR) was 70 STB/MMCFD at the field development stage and this CGR is considered to be quite high for a dry gas well.

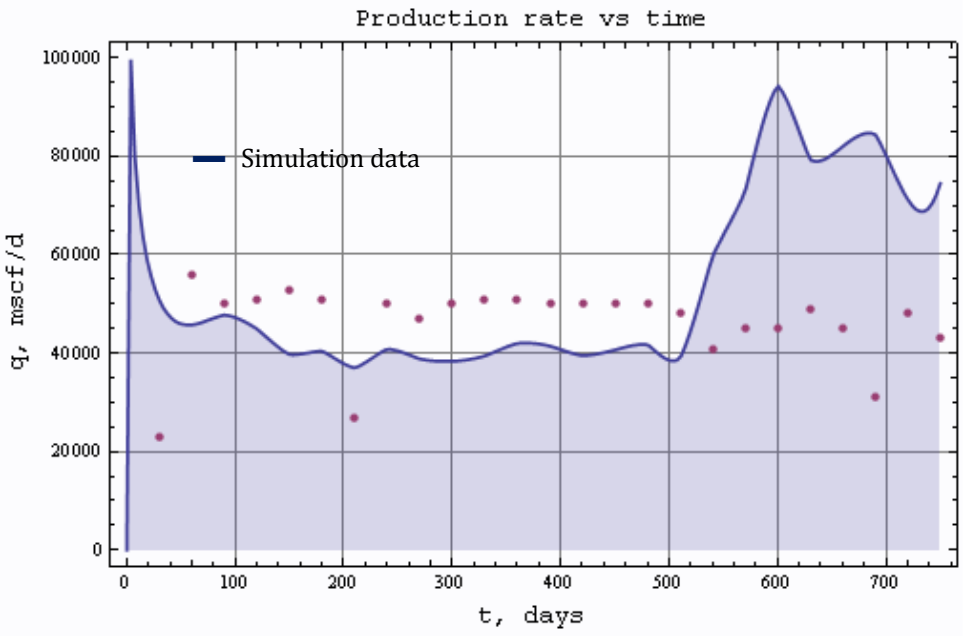

Fig. 4.4—Production rate versus time for well SA-1

As a reservoir is depleted and a well has less pressure near the wellbore area, condensate drop-out may occur and limit gas flow. In addition, I noticed that the casing diameter is large at the perforation and tubing does not reach to the perforation area. This may cause a liquid loading problem as the reservoir is depleted and large cross-sectional flow area lowers gas velocity near the perforation area. Before the 17th month we can find almost constant gas rates in both cases.

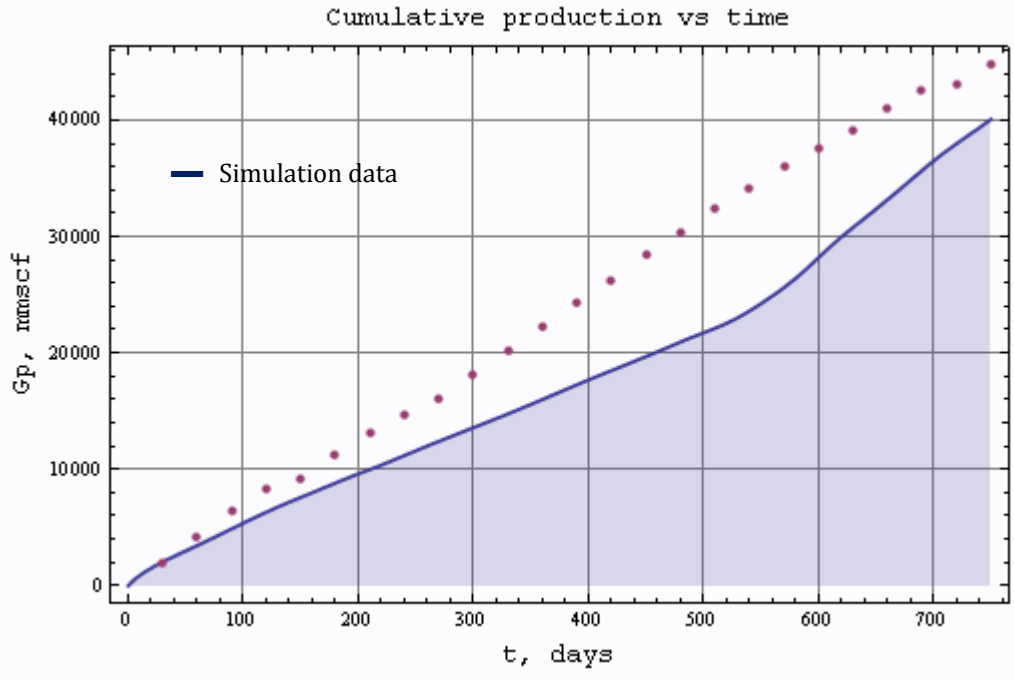

Fig. 4.5—Cumulative production versus time for well SA-1

In cumulative production as shown in Fig. 4.5, simulation data seems to differ from field data but at the end of production the gap between simulation data and field data decreases. Using a constant condensate gas ratio from PVT data at the field development stage might cause this gap.

SA-2: In the case of SA-2, we cannot see really stabilized J_D in the field case, as shown in **Fig. 4.6**. J_D in the field case seems to be up and down. After comparing simulation data, the transient period might be from 1st to 3rd or 4th month and the JD ranges between 0.3 and 0.45. Although J_D is not really stabilized, pseudo-steady state regime might begin from the 4th month, because J_D fluctuates in a certain range (0.25 to 0.35) and it is difficult to find a stabilized J_D in reality.

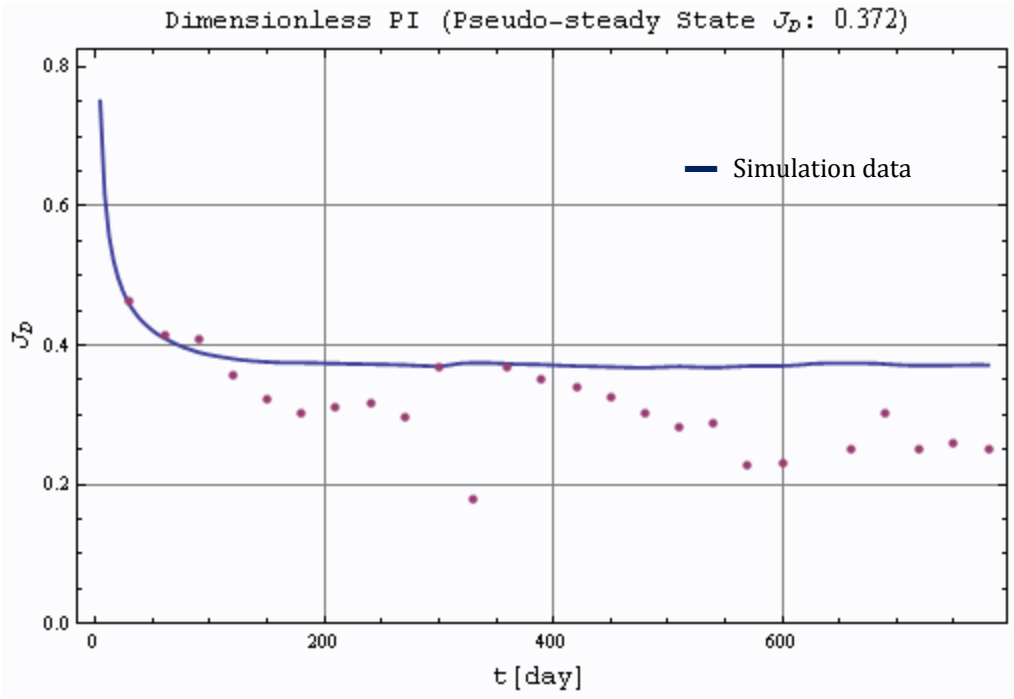

Fig. 4.6—Dimensionless productivity index versus time for well SA-2

Production rate and cumulative production of SA-2 is well matched with the "Gas Acid" simulation data. Compared to SA-1, the discrepancy in cumulative production between field data and simulation data is greatly decreased (12.5% to 6.25%). Production rate and cumulative production of SA-2 are depicted in **Figs. 4.7** and **4.8**.

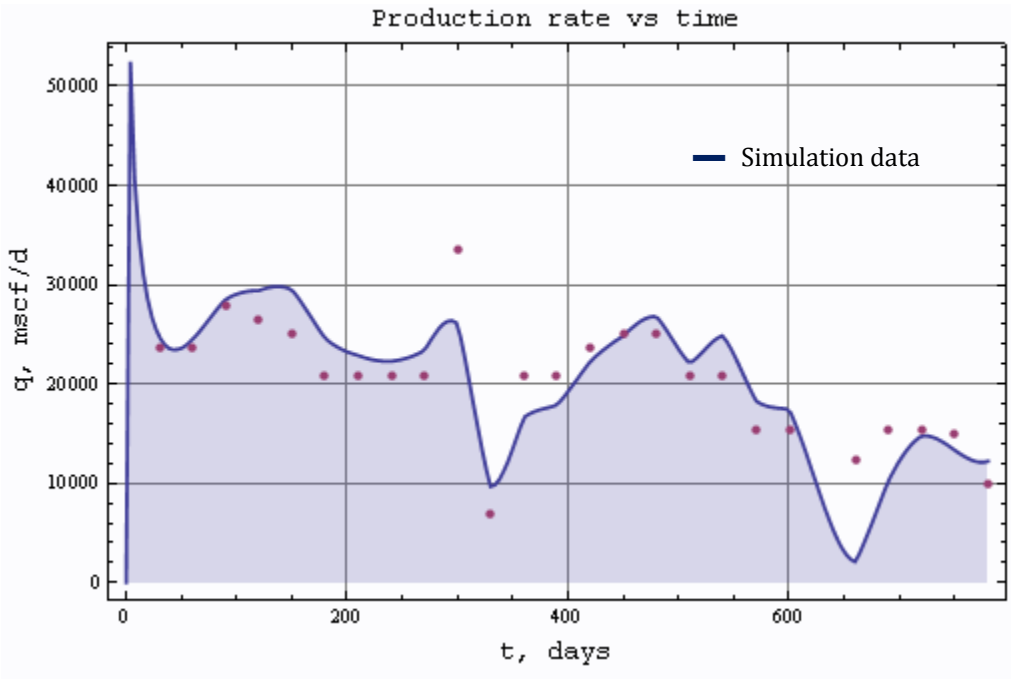

Fig. 4.7—Production rate versus time for well SA-2

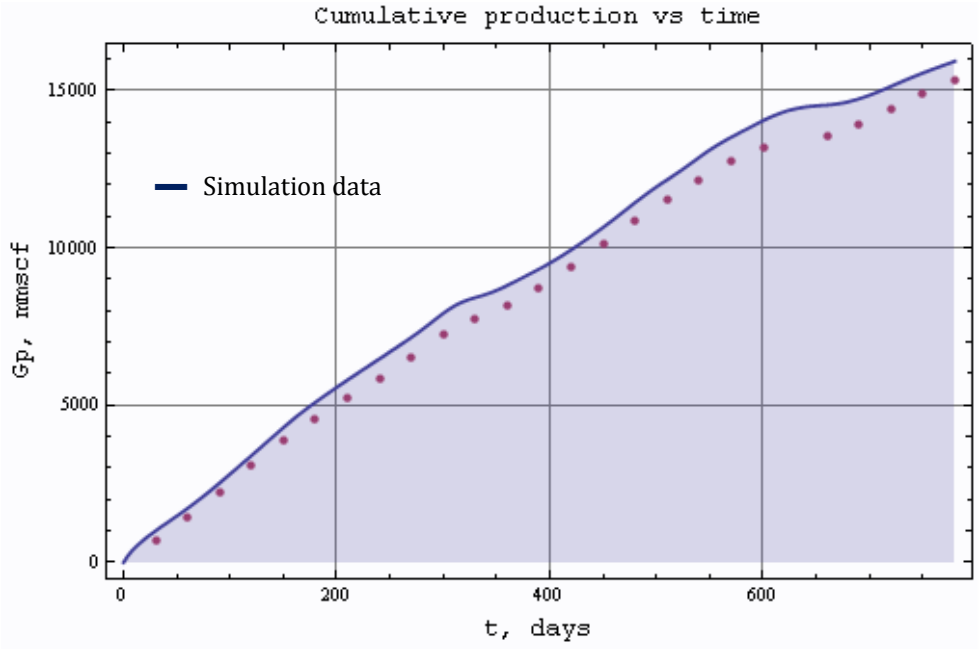

Fig. 4.8—Cumulative production versus time for well SA-2

CHAPTER V

DISCUSSION

5.1 The Possible Reasons for Sudden Drop of PI

A sudden change in the PI of well SA-1 can have several explanations, such as condensate bank, conductivity reduction in fractured area, and liquid loading. In this chapter, I will discuss those possibilities.

5.1.1 Condensate Bank

Bonorgzadeh and Graingarten (2004) noted that when bottomhole flowing pressure falls below the dewpoint in a gas/condensate reservoir, retrograde condensation occurs, and a bank of condensate builds up around the producing well. This results in reduced gas mobility. **Table 5.1,** provided by Olaberinjo *et al*. (2006), shows different gas condensate compositions, classifying rich gas condensate and lean gas condensate to evaluate differences in flow rates for them. Rich gas condensate has a very high mole % of C7+ compared to lean gas condensate, which has only 8.21% of C7+.

TABLE 5.1 – Gas condensate feed composition

Component	Mole %-Rich gas condensate	Mole %-Lean gas condensate
C_1 (Light)	58.77	73.190
C_2-C_6 (Intermediate)	18.33	15.920
C_{7+} (Heavier)	21.76	08.210
N_2	00.21	00.310
CO_2	00.93	02.370
Total mole	100.00	100.00

TABLE 5.2-Gas compostion for well SA-1	
Component	Well Stream Mole%
Nitrogen	7.6
Carbon Dioxide	0.93
Hydrogen Sulfide	0.00
Methane	72.61
Ethan	7.79
Propane	3.45
i - Butane	0.63
n - Butane	1.30
i - Pentane	0.44
n - Pentane	0.49
Hexanes	0.59
Heptanes	0.73
Octanes	0.74
Nonanes	0.61
Decanes Plus	2.09
Total	100.00

PVT data for well SA-1 (see **Table 5.2**) shows that C7+ is less than 5 mole % of gas components, so the type of fluid in well SA-1 is more likely to be lean gas condensate and there is no clear indication of possibility in occurrence of condensate blockage based on gas composition used in Olaberinjo's research. Algahamdi (2005) has performed a flash point calculation and run PVTsim to draw the phase envelop for well SA-1, as shown in **Fig. 5.1**. **Fig. 5.1** demonstrates that liquid will be dropped out at 270°F and 5,650 psi and this can be used to determine whether liquid dropout would occur within the operational parameters, such as flowing bottomhole pressure. In the bottomhole pressure history of well SA-1 before the sudden PI drops, the well was producing gas with around 6400 to 5800 psi FBHP, indicating a very low possibility of liquid dropout near the wellbore area. However, as PI rapidly decreased after 18 months of production, it could have caused the condensate bank and additional PI drop as FBHP decreased.

However, it was clear that a root cause of PI drop would not be condensate bank due to pressure drop below the dew point. Comparing the gas condensate ratios of SA-1 and SA-2, SA-1 has the smaller value of gas condensate ratio and the SA-2 well has not experienced sudden PI drops. This also demonstrates that condensate bank may not be the root cause of the PI reduction that occurred in SA-1.

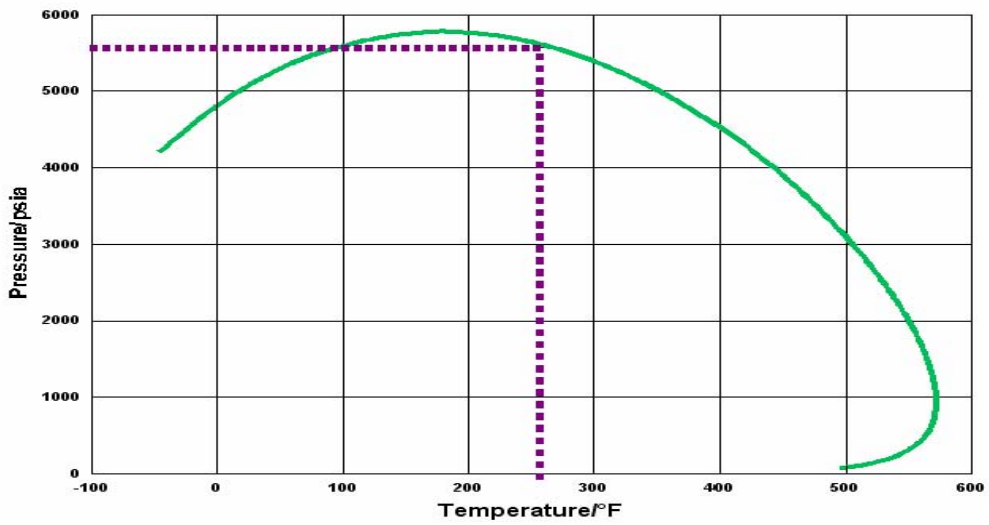

Fig. 5.1-Phase envelope diagram generated by PVTsim at a given gas composition[21]

5.1.2 Liquid Loading

Previous discussion demonstrated that there is a very low probability of the occurrence of condensate bank near wellbore area as FBHP was always higher than the dewpoint. However, as gas flows through the tubing to the surface, fluids will meet the dew point in the middle of the tubing and condensate will be formed. According to Dotson and Nunez-Paclibon (2007), gas wells cease producing as reservoir pressure depletes and gas velocity decreases. Below the critical rate, liquids cannot be lifted from the wellbore and instead, settle to the bottom. As liquid loading probability causes the

reduction in PI followed by reduced gas production, I have overviewed completion constraint and production. It is very clear that gas production was reduced rapidly but it could not be verified whether or not liquid production decreased due to the lack of condensate and water production data. Completion data shows that 6.094 in. casing with perforation does reach to the bottom but 4.778 in. tubing was installed at the depth of 3192 ft above the casing. A very large inner diameter of casing at the perforation can reduce the gas velocity significantly so condensate may accumulate at the bottom, thus limiting the gas flow rates from the reservoir. Inferring from those facts, liquid loading may be the root cause of the PI reduction that occurred in SA-1.

5.1.3 Conductivity Reduction

Nasr-El-Din *et al.* (2002) have demonstrated rock embedment strength before and after exposure to acid by making measurements on the Khuff formation using Brinell hardness methods. Rock strength was reduced by 20% to 63% after acidizing as shown below in **Table 5.3**. If rock embedment strength decreases, then acid fracture conductivity can be deteriorate. Abass H.H. *et al.* (2006) also said that productivity decline in an acid-fractured well is an integrated response of the elastic, plastic, and creeping response to applied stress and about 30%-40% of production rate decline occurs during a short time as a result of creeping of the acid-softened carbonate formation. The sudden drop of SA-1 might be caused by closure of some part of the fracture and severe deterioration of the fracture conductivity.

TABLE 5.3-Hardness information before and after acidizing Khuff core samples.

Lithology	Rock Embedment Strength, psi	
	Before	After
Limestone	70,425	50,784
	51,072	31,494
	59,041	39,040
Dolomite	62,027	49,324
	129,988	47,647

CHAPTER VI

SUMMARY AND CONCLUSIONS

6.1 Summary

The primary objective of this research is to develop the program called “Gas Acid” for evaluation of acid fracturing. The DVS method is used to calculate well productivity of both a transient regime and a pseudosteady-state regime. Typically, the DVS method is used for various well/fracture configurations, but I only use the section for vertical well with vertical fracture because no deviated wells were studied for acid treatment in this research. The Nierode-Kruk correlation was used to estimate acid fracture conductivity and fracture conductivity value was used to determine the dimensionless productivity index with two-variable interpolation function and a given time. The combination of the obtained dimensionless productivity index with material balance allowed us to forecast the production of acid fractured wells. Originally “Gas Acid” was only applicable to dry gas reservoirs, because single phase assumption is used in the DVS method and conventional gas material balance is used to forecast production. However, we obtained good agreement for a wet gas reservoir, as well, by converting condensate to gas amount. Thus, if condensate to gas ratio is available, “Gas Acid” can evaluate the performance of a wet gas range reservoir as well as a dry gas range reservoir.

6.2 Conclusions

On the basis of my research, the following conclusions are offered:

1. The “Gas Acid” program will allow us to predict performance of the acid fracturing well by providing dimensionless productivity index, flow rate, cumulative production, average reservoir pressure with given reservoir geometry and the well completion scheme.
2. From the simulated performance data, we can find optimum parameters and fracture dimensions, which we should target for a given acid volume. To consider economic aspects, the most efficient acid volume can also be determined by simulation.
3. Field application shows that there is reasonable agreement between simulation data by “Gas Acid” and field data. After accounting for the additional mass of gas “hidden” in the produced condensate, “Gas Acid” is available not only for dry gas but also wet gas range reservoirs. For improving accuracy, further refinement of the material balance should be considered.
4. Possible reasons for the sudden drop of the productivity index in the SA-2 well are the liquid loading and fracture conductivity deterioration. Condensate bank may not be the reason in this case.

NOMENCLATURE

Variables

A	=	reservoir drainage area, ft^2
c_t	=	total compressibility, psi^{-1}
c_{trad}	=	conversion factor
c_x	=	position of the center of the source in x direction, ft
c_y	=	position of the center of the source in y direction, ft
c_z	=	position of the center of the source in z direction, ft
f	=	1D solution to the flow equation
h_f	=	fracture height, ft
J_D	=	dimensionless productivity index
$J_{D,\,trad}$	=	traditional definition of dimensionless productivity index
k	=	permeability, reference permeability, md
k_x	=	directional permeability in x direction, md
k_y	=	directional permeability in y direction, md
k_z	=	directional permeability in z direction, md
p	=	pressure, psi
p_i	=	initial pressure, psi
p_{wf}	=	well flowing pressure, psi
$p_{\delta D}$	=	dimensionless pressure due to instantaneous source
PI	=	productivity index, STB/d/psi
p_{uD}	=	dimensionless pressure due to continuous source
t	=	time

t_D	=	dimensionless time
t_{DA}	=	dimensionless time with regard to reference drainage volume
$t_{DA,\ trad}$	=	dimensionless time with regard to fracture half-length
V	=	injected acid volume, ft^3
w	=	fracture width, ft
w_x	=	source width in x direction, ft
w_y	=	source width in y direction, ft
w_z	=	source width in z direction, ft
X	=	volumetric dissolving power
x_D	=	dimensionless length in x direction, x/xe
x_e	=	length of outer box, ft
y_D	=	dimensionless width in y direction, y/ye
x_f	=	fracture half length, ft
y_e	=	width of the outer box, ft
z_D	=	dimensionless height in z direction, z/ze
z_e	=	height of the outer box, ft

Greek Symbols

ϕ	=	porosity, fraction
μ	=	viscosity, cp
σ	=	net closer pressure, psi

REFERENCES

Abass, H.H., Al-Mulhem, A.A., Alqam M.S., and Mirajuddin, K.R. 2006. Acid Fracturing or Proppant Fracturing in Carbonate Formation? A Rock Mechanic's View. Paper SPE 102590 presented at the 2006 SPE Annual Technical Conference and Exhibition, San Antonio, TX, 24-27 September.

Algahmdi A. 2005. *Evaluation of Acid Fracturing Based on the Acid Fracture Number Concept*. MS thesis, Texas A&M University, College Station, TX.

Al-Hussainy, R. and Ramey, H. J. 1965. Application of Real Gas Flow Theory to Well Testing and Deliverability Forecasting. Paper SPE 1243 presented at SPE Annual Fall Meeting held in Denver, CO., Oct. 3-6.

Al-Qahtani, M.Y, and Rahim, Z.M. 2001. A Mathematical Algorithm for Modeling Geomechanical Rock Properties of the Khuff and Pre-Khuff Reservoir in Ghawar Field. Paper SPE 68194 presented at the 2001 SPE Middle East Oil Show, Manama, Bahrain, 17-20 March.

Amini, S. 2007. Development and Application of the Method of Distributed Volumetric Sources to the Problem of Unsteady State Fluid Flow in Reservoirs. PhD dissertation, Texas A&M University, College Station, TX.

Bartko, K.M., Nasr-El-Din, H.A., Rahim, Z., and Al-Muntasheri, G.A. 2003. Acid Fracturing of a Gas Carbonate Reservoir: The Impact of Acid Type and Lithology on Fracture Half Length and Width. Paper SPE 84130 presented at the 2003 SPE Annual Technical Conference and Exhibition, Denver, CO, 5-8 October.

Bozorgzadeh, M., and Gringarten, A.C. 2004. Condensate-Bank Characterization From Well-Test Data and Fluid PVT Properties. Paper SPE 89904 presented at the 2004 SPE Technical Conference and Exhibition, Houston, TX, 26-29 September.

Dotson, B. and Nunez-Paclibon E. 2007. Gas Well Liquid Loading From the Power Perspective. Paper SPE 110357 presented at the 2007 SPE Annual Technical Conference and Exhibition, Anaheim, CA, 11-14 November.

Economides, M. J. and Martin, T. 2007. *Modern Fracturing-Enhancing Natural Gas Production*. Houston, TX: ET Publishing.

Economides, M.J. and Nolte, K.G. 1998. *Reservoir Stimulation*, 3rd Edition. Houston, TX: Schlumberger Educational Services.

Economides, M., Oligney, R. and Valkó, P. 2002. *Unified Fracture Design-Bridging the Gap between Theory and Practice*. Alvin, TX: Orsa Press.

Fekete Associates Inc. 2005. FAST RTA Technical Documentation. Calgary, Canada

: Fekete Associates Inc

Guo, Boyun and Ghalambor, Ali. 2005. *Natural Gas Engineering Handbook*. Houston, TX: Gulf Publishing Company.

Helmy, M. W. and Wattenbarger, R. A. 1998. Simplified Productivity Equations for Horizontal Wells Producing at Constant Rate and Constant Pressure. Paper SPE 49090 presented at the 1998 SPE Annual Technical Conference and Exhibition, New Orleans, LA, 27-30 September.

Jin X. 2008. *Gas Deliverability Using the Method of Distributed Volumetric Sources.* MS thesis, Texas A&M University, College Station, TX.

Kalfayan, L.J. 2007. Fracture Acidizing: History, Present State, and Future. Paper SPE 106371 presented at the 2007 SPE Hydraulic Fracturing Technology Conference, College Station, TX, 29-31 January.

Nasr-El-Din, H.A., Al-Mutairi, S.H., Al-Malki, M., Metcalf, S., and Wallace, W. 2002. Stimulation of a Deep Sour Gas Reservoir Using Gelled Acid. Paper SPE 75501 presented at the 2002 SPE Gas Technology Symposium, Calgary, Canada, 30 April-2 May.

Nierode, D.E., and Kruk, K.F. 1973. An Evaluation of Acid Fluid Loss Additives, Retarded Acids, and Acidized Fracture Conductivity. Paper SPE 4549 presented at the 1973 SPE 48th Annual Fall Meeting, Las Vegas, NV, 30 September- 3 October.

Olaberinjo, A.F., Oyewola, M.O., Adeyanju, O.A., Alli, O.A., Obiyemi, A.D. and Ajala, S.O. 2006. KPIM of Gas/Condensate Productivity: Prediction of Condensate/Gas Ratio Using Reservoir Volumetric Balance. Paper SPE 104307 presented at the 2006 SPE Eastern Regional Meeting, Canton, OH, 11-13 October.

Rahim, Z.M., and Al-Qahtani, M.Y. 2001. Sensitivity Study on Geomechanical Properties to Determine Their Impact on Fracture Dimensions and Gas Production in the Khuff and Pre-Khuff Formations Using a Layered Reservoir System Approach, Ghawar Reservoir, Saudi Arabia. Paper SPE 72142 presented at the 2001 SPE Asia Pacific Improved Oil Recovery Conference, Kuala Lumpur, Malaysia, 8-9 October.

Romero, D. J., Valkó, P. P. and Economides, M. J. 2002. Optimization of the Productivity Index and the Fracture Geometry of a Stimulated Well with Fracture Face and Choke Skins. Paper SPE 73758 presented at the 2002 International Symposium and Exhibition on Formation Damage Control, Lafayette, LA, 20-21 February.

Valkó, P. P. and Amini, S. 2007. The Method of Distributed Volumetric Sources for Calculating the Transient and Pseudo-steady State Productivity of Complex Well-Fracture Configurations. Paper SPE 106729 presented at the 2007 SPE Hydraulic Fracturing Technology Conference, College Station, TX, 29-31 January.

APPENDIX A

NATURAL GAS CORRELATIONS

In “Gas Acid” program, gas properties such as compressibility factor, viscosity, gas compressibility are calculated by related subroutine and these values allow us to obtain real gas pseudopressure to analyze gas production. Natural gas is a complex mixture of light hydrocarbons with a minor amount of inorganic compounds, it is always desirable to find the composition of the gas through measurements (Guo *et al*., 2005). Once the gas composition is known, gas properties can usually be estimated using established correlations with confidence. Gas specific gravity and mole fraction of inorganic compounds are inputs for “Gas Acid” program and these are used for calculating gas properties at given pressure and temperature. In this section, I will explain which correlation is used and show the graphs directly from “Gas Acid” program.

We use Beggs and Brill (1974) correlation to calculate compressibility factor (Guo *et al*., 2005). This is deviation from ideal gas. **Fig. A.1** shows compressibility factor versus pressure at given temperature.

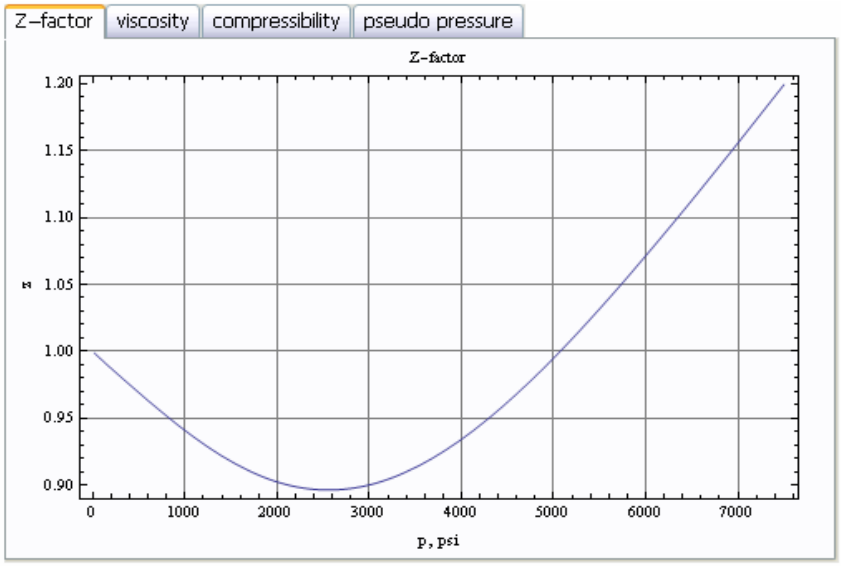

Fig. A.1-Compressibility factor vs Pressure at T=280°F

The gas viscosity correlation of Carr, Kobayashi, and Burrows (1954) involves a two-step procedure (Guo *et al*., 2005): the gas viscosity at temperature and atmospheric pressure is estimated first from gas specific gravity and inorganic compound content. The atmospheric viscosity value is then adjusted to pressure conditions by means of a correction factor on the basis of reduced temperature and pressure state of the gas. **Fig. A.2** show gas viscosity versus pressure.

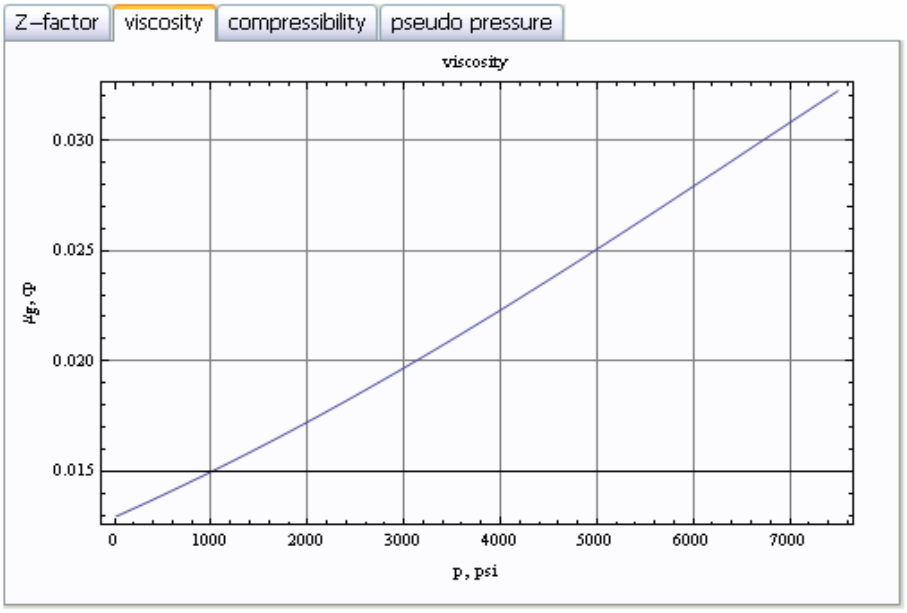

Fig. A.2-Viscosity vs Pressure at T=280°F

Gas compressibility is calculated by the equation blew:

$$c_g = -\frac{1}{V}\frac{\partial V}{\partial p} = \frac{1}{p} - \frac{1}{z}\frac{\partial z}{\partial p}$$

Fig. A.3 show us Gas compressibility versus pressure.

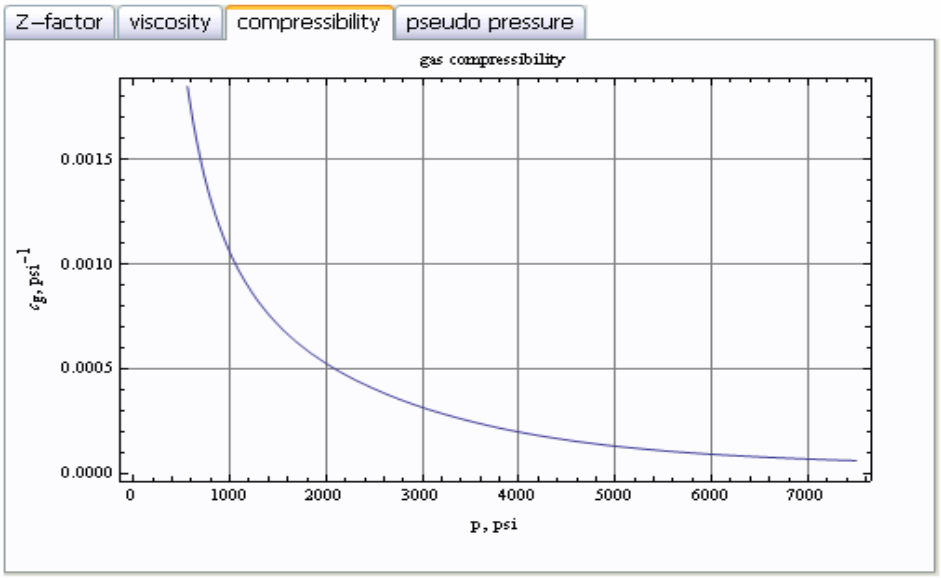

Fig. A.3-Gas compressibility factor vs Pressure at T=280°F

Real gas pseudopressure m(p) is defined as:

$$m(p) = \int_{p_b}^{p} \frac{2p}{\mu z} dp$$

Where p_b is the base pressure (14.7psi). the psudopressure is considered to be a "pseudoproperty" of gas because it depends on gas viscosity and compressibility factor, which are properties of the gas. The pseudopressure is widely used for mathematical modeling of IPR of gas wells. Determination of the pseudopressure at a given pressure requires knowledge of gas viscosity and z-factor as functions of pressure and temperature. **Fig. A.4** shows pseudopressure versus real pressure at given temperature.

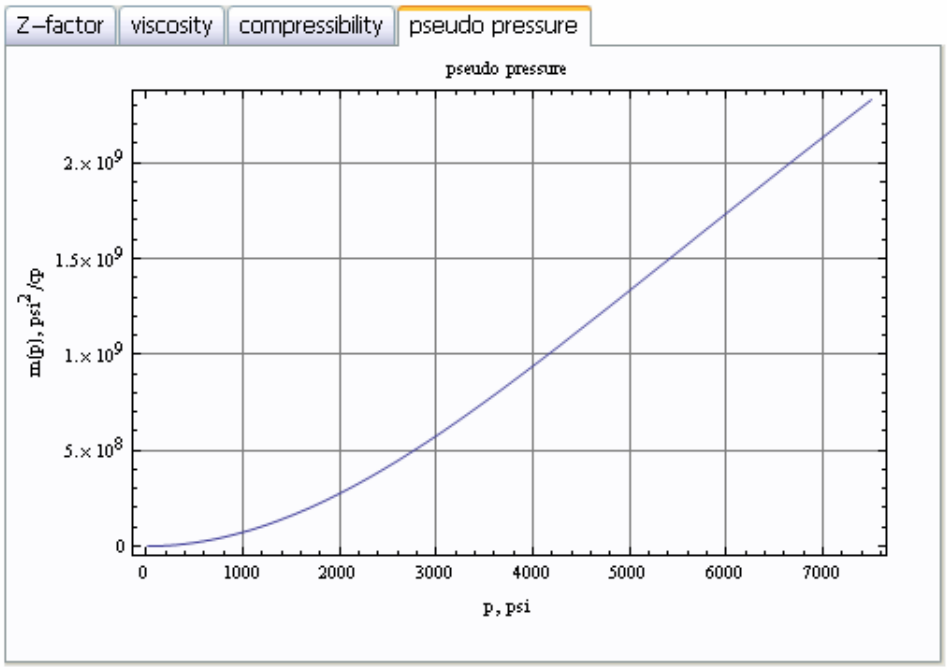

Fig. A.4-Pseudopressure vs Real pressure at T=280°F

APPENDIX B

DIMENSIONLESS PRODUCTIVITY INDEX FOR CONSTANT RATE

The further use of DVS method was developed by Valkó *et al*. (2007) as a way to predict productivity of complex well/fracture systems.

In production engineering, the productivity index is defined as the ability of the reservoir to produce hydrocarbon per unit pressure drop in the reservoir (volume/time/pressure).

$$J = \frac{q}{p_{avg} - p_{wf}} \qquad (2.3)$$

In which

q = Flow Rate

p_{avg} = Average Reservoir Pressure

p_{wf} = Well Flowing Pressure

Introducing the Dimensionless parameters as the followings the expression for the Dimensionless productivity index would be obtained.

$$p_{D,trad} = \frac{2\pi kh}{qB\mu}(p_i - p) \qquad (2.4)$$

$$J_D = \frac{\mu B}{2\pi kh} J \qquad (2.5)$$

With:

p_i = Initial Reservoir Pressure

k = Reservoir Permeability

h = Reservoir Thickness

B = Formation Volume Factor

μ = Fluid Viscosity

Combining Eqs. 2.1 through 2.3 we have:

$$J_D = \frac{1}{p_{D,trad} - p_{D,avg,trad}} \quad \text{..... (2.6)}$$

Assuming a constant and small compressibility during depletion we can write:

$$c_t = -\frac{1}{V}\frac{\partial V}{\partial p} \quad \text{..... (2.7)}$$

$$V = \phi Ah \quad \text{..... (2.8)}$$

$$\frac{\partial p}{\partial V} = \frac{1}{\phi Ahc_t} \quad \text{..... (2.9)}$$

$$\Delta p = p_i - p_{avg} = \frac{\Delta V}{\phi Ahc_t} = \frac{N_p B}{\phi Ahc_t} = \frac{qBt}{\phi Ahc_t} \text{ (Constant flow rate production) ..... (2.10)}$$

Using the definition for dimensionless pressure and applying it on Eq. 2.8 we have:

$$p_{D,avg,trad} = 2\pi \frac{kt}{\phi\mu c_t A} = 2\pi t_{DA} \quad \text{..... (2.11)}$$

Where:

$$t_{DA} = \frac{kt}{\phi\mu c_t A} \text{ (Dimensionless time based on drainage area) ..... (2.12)}$$

Combination of Eq. 2.11 and 2.6 would lead us to an expression correlating the dimensionless productivity index as a function of dimensionless pressure and dimensionless time (Eq. 2.13)

$$J_D = \frac{1}{p_{D,trad} - 2\pi t_{DA}} \quad \text{..... (2.13)}$$

Based on the new dimensionless variables defined in the DVS method, we will get

$$J_D = \frac{1}{2\pi c_{trad}(p_{uD} - t_D)} \quad \text{..... (2.14)}$$

where,

$$c_{trad} = \frac{z_e\sqrt{k_x k_y}}{L\,k} \quad \text{..... (2.15)}$$

$$p_{uD} = \int_0^{t_D} p_{\delta D}(t_D^{'}).dt_D^{'} \quad \text{..... (2.16)}$$

$$t_D = \frac{k}{\phi\mu c_t L^2}t \quad \text{..... (2.17)}$$

$$k = (k_x k_y k_z)^{\frac{1}{3}}$$
$$L = (x_e y_e z_e)^{\frac{1}{3}} \quad \text{(k and L are reference permeability and length) ..... (2.18)}$$

There is a relationship between t_{DA} and t_D

$$t_{DA} = c_{trad}\, t_D \quad \text{..... (2.19)}$$

The dimensionless productivity index is time dependent in the transient flow regime and constant in the pseudo-steady state.

In field units, the productivity index is expressed as

$$PI = \frac{z_e\sqrt{k_x k_y}}{141.2B\mu} J_{D,trad} \quad \text{..... (2.20)}$$

Where k is in md, μ in cp, B in resBBL/STB, q in STB/D, pwf and pi in psi, t in hr, ct in 1/psi, φ is dimensionless and PI is in (STB/D/psi).

APPENDIX C

DATA ANALYSIS

Table C.1-Summary of results obtained from PROSPER for SA-1				
Month	FWHP, psig	Average reservoir pressure, psi	Skin	FBHP, psi
1	4970	7469	-4.23	6442
2	4788	7436	-6.93	6410
3	4692	7402	-6.60	6278
4	4703	7370	-6.83	6278
5	4763	7357	-6.98	6344
6	4663	7325	-6.83	6278
7	4822	7296	-5.10	6312
8	4625	7272	-6.78	6179
9	4621	7250	-6.54	6179
10	4546	7218	-6.60	6147
11	4491	7188	-6.66	6081
12	4452	7155	-6.54	5981
13	4424	7124	-6.47	5949
14	4393	7093	-6.47	5949
15	4359	7060	-6.47	5883
16	4335	7030	-6.47	5816
17	4330	6998	-6.47	5839
18	3927	6971	-4.56	5349
19	3637	6943	-4.10	5003
20	3150	6918	-2.85	4428
21	3311	6895	-4.10	4687
22	3255	6865	-3.22	4543
23	3157	6840	-0.01	4400
24	3281	6833	-3.84	4629
25	3201	6807	-3.22	4485

Table C.2-Summary of results obtained from PROSPER for SA-2				
Month	FWHP, psig	Average reservoir pressure, psi	Skin	FBHP, psi
1	4502	7505	-6.95	6290
2	4362	7488	-6.70	6130
3	4080	7471	-6.66	5801
4	3960	7454	-6.30	5661
5	3893	7437	-6.00	5583
6	4067	7420	-5.80	5796
7	4110	7403	-5.90	5846
8	4100	7386	-5.95	5834
9	4009	7369	-5.75	5729
10	3843	7352	-6.40	5529
11	4495	7335	-3.50	6427
12	4252	7318	-6.40	6010
13	4162	7301	-6.25	5906
14	3924	7284	-6.15	5622
15	3767	7267	-6.03	5432
16	3635	7250	-5.80	5273
17	3818	7233	-5.55	5501
18	3650	7216	-5.65	5299
19	3908	7199	-4.70	5637
20	3924	7182	-4.75	5656
21	N/A	N/A	N/A	N/A
22	4615	7182	-5.10	6490
23	4238	7165	-5.80	6022
24	3998	7148	-5.10	5744
25	4048	7131	-5.25	5802
26	4074	7100	-5.10	5844

APPENDIX D

USER MANUAL FOR GAS ACID

PDF form of the user manual for “Gas Acid” program is available.

VITA

Name: Jaehun Lee

Permanent Address: Harold Vance Department of
Petroleum Engineering,
3116 TAMU,
College Station, TX 77843-3116

Email Address: tigerleebart@hotmail.com

Education: B.S., Geoenvironmental System Engineering,
Hanyang University, March 2006
M.S., Petroleum Engineering,
Texas A&M University, August 2009